Electrochemical Testing of Aluminum-Lithium Alloys 2050, 2195, and the Current Aerospace Industry Standard 7075 to Measure the Galvanic Corrosion Behavior with Ti-6Al-4V

A Senior Project
Presented to
the Faculty of the Materials Engineering Department
California Polytechnic State University, San Luis Obispo

In Partial Fulfillment
of the Requirements for the Degree
Bachelor of Science, Materials Engineering

by
Trent Duncan, Kevin Knight
June 2015

Abstract

This project aimed to characterize the electrochemical behavior of four different aluminum alloys, and determine how much galvanic corrosion would occur when each alloy was coupled to Ti-6Al-4V. The particular alloys tested were 2050-T3, 2050-T852, 2195-T852, and 7075-T7352. These alloys were tested to determine the effects of aging, and adding lithium, to the corrosion behavior of aluminum alloys. Potentiodynamic polarization curves were generated using the Parstat 2273 potentiostat in accordance with ASTM standard G5, and corrosion analysis software was used to produce Tafel fit lines, which determined the open circuit potential (E_{corr}) of each sample. Nine tests were run on each alloy and proper statistical analysis was used to determine an E_{corr} value. These potential values were used to develop a galvanic series in accordance with ASTM standard G82 to characterize the corrosion behavior of the aluminum alloys when coupled to Ti-6Al-4V. The differences between average E_{corr} values of each aluminum alloy and Ti-6Al-4V were calculated to predict the extent of galvanic corrosion that would occur. The differences in E_{corr} values were found to be 281.21 mV for 2050-T3, 319.02 mV for 2050-T852, 300.72 mV for 2195-T852, and 439.45 mV for 7075-T7352.

Key Words: Galvanic Corrosion, Aluminum-Lithium Alloys, Ti-6Al-4V, 2195, 2050, 7075, Electrochemical Potential, Potential Difference, Structural Aerospace Components, Materials Engineering

Acknowledgements

We would like to thank Kyle Logan and Mark Timko from Weber Metals (Paramount, CA) for supplying us with the metals needed as well as for their sponsorship and support throughout the duration of this project. In addition, we would also like to acknowledge Luka Dugandzic from Dugandzic Design (San Luis Obispo, CA) for machining the corrosion samples to the appropriate dimensions. Lastly, we would like to thank our advisor, Professor Blair London, for his guidance and wisdom throughout this past year.

Table of Contents

List of Figures

List of Tables

1. Introduction

1.1 Project Overview

Weber Metals (Paramount, CA) is a forging supplier that specializes in manufacturing structural aircraft components made of aluminum and titanium alloys. In the aerospace industry, 7075 aluminum and Ti-6Al-4V are common alloys that are used for aircraft parts, and these materials are often in contact with one another. Since aluminum and titanium are dissimilar metals, coupling them causes a situation in which galvanic corrosion can occur. Although 7075 aluminum has a high strength-to-density ratio and is tough for an aluminum alloy, aluminum-lithium alloys 2195 and 2050 possess better mechanical properties and look promising as effective substitutes for 7075 aluminum. For this project, a potentiostat will be used to measure the electrochemical potential of 7075, 2195, 2050, and Ti-6Al-4V in a marine environment. From these electrochemical potential measurements, a galvanic series will be developed using ASTM Standard G82 to determine how well the aluminum-lithium alloys compare to 7075. This data will be used by Weber Metals to show their customers all the benefits of purchasing parts made of high-performance aluminum-lithium alloys in order to justify higher costs.

1.2 Background Information

1.2.1 Application

Aircraft are made up of multiple materials, each suited for a different application. Both aluminum and titanium alloys are used to make up the structural components of both military and commercial aircraft. These alloys are used due to their high specific strength and high specific stiffness. The approximate location of parts made of each alloy, as well as their percentage of the plane by weight can be seen in Figure 1.

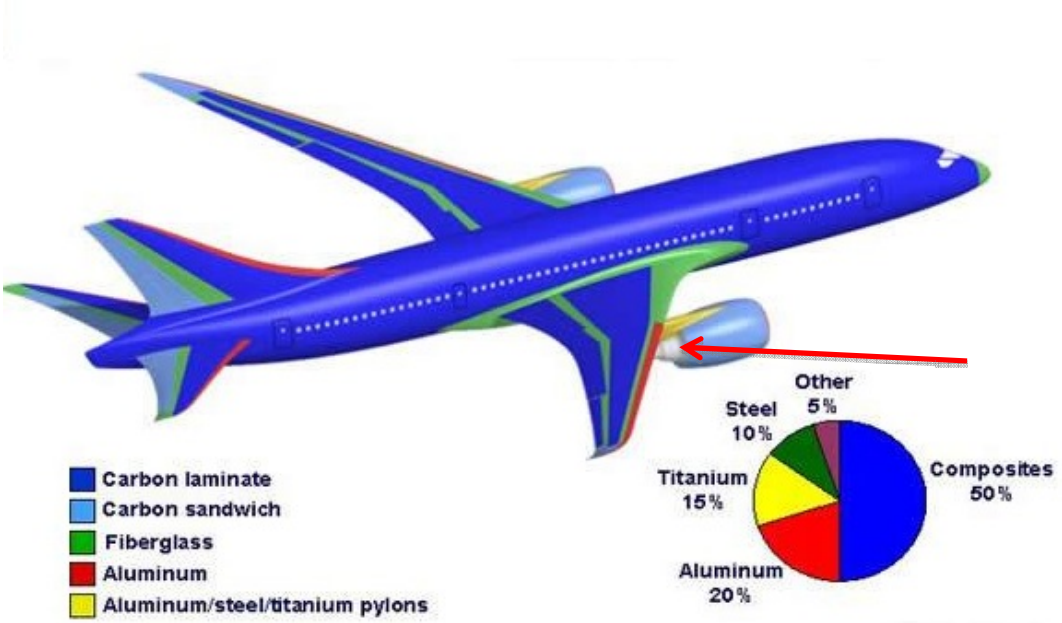

Figure 1: Aluminum makes up 20% of the weight of the aircraft while titanium makes up 15%. It can also be noted that the aluminum (red) and titanium (yellow) come into contact with each other.[1]

A current challenge in the aeronautical field is the reduction in weight of aircraft structures. The properties that have the greatest impact on reducing the weight in aircraft are density, yield strength, tensile strength, stiffness, and damage tolerance (Figure 2).

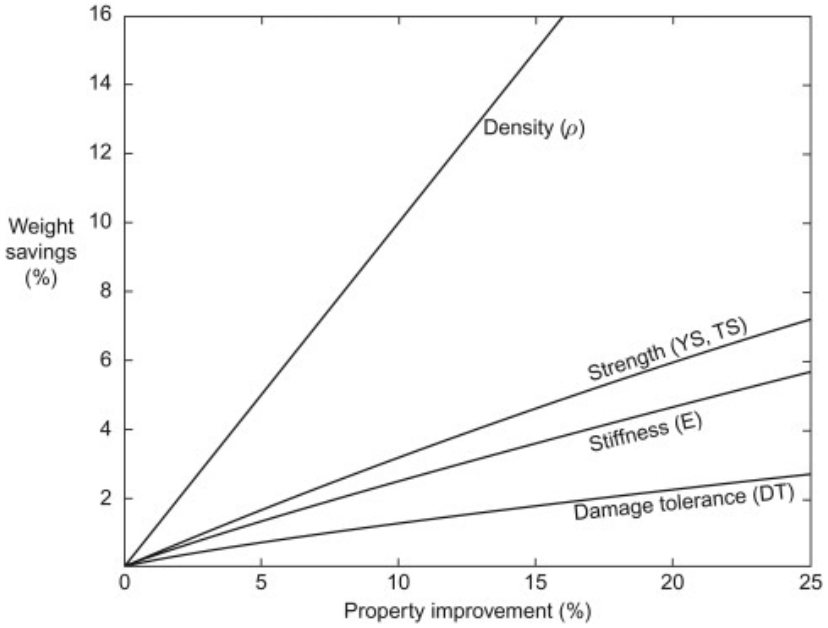

Figure 2: Effects of property improvements on the overall weight savings of the aircraft.[2]

Decreasing the density produces the best weight savings, but increasing the strength, stiffness, and damage tolerance also reduces the weight by allowing the design to use less material. The combination of being lightweight while still remaining strong is why 7075 and Ti-6Al-4V are widely used throughout the aerospace industry.

1.2.2 Aluminum Alloys

Aluminum alloys are used for a variety of engineering applications but excel specifically in structural aerospace applications because of their high strength-to-density ratios. One specific aluminum alloy is 7075, which is a wrought, heat-treatable alloy consisting of primary alloying elements zinc, magnesium, and copper (Table I).

Table I: Composition of 7075 (wt%)[3]

Alloying Element	Zn	Mg	Cu	Cr	Al
Wt%	5.6	2.5	1.6	0.23	Bal

7075 was introduced by Alcoa in 1943 and has been the most used alloy in the aerospace industry since. It is used primarily because of its high specific strength and moderate toughness. The addition of chromium increases the stress corrosion cracking resistance of the alloy. Properties like these can be influenced by the effect of aging. Two common aluminum temper designations are T3 and T852. Aluminum alloys that are T3 conditioned are solution heat treated, cold worked, and naturally aged while aluminum alloys that are T852 conditioned are solution heat treated, stress-relieved by compressing to produce a permanent set of 1-5%, and then artificially aged.

1.2.3 Aluminum-Lithium Alloys

Adding lithium to aluminum alloys has shown an improvement in the mechanical properties of the alloys. Every wt% of lithium added to aluminum results in a 3% decrease in density, and a 6% increase in Young's modulus.[4] However, there is a limit in the amount of lithium that can be added to Al-Li alloys. It was found that contents of 2 wt% Li or more are linked to several disadvantages; such as, a tendency for strongly anisotropic mechanical properties, low short-transverse ductility and fracture toughness, and a loss of toughening. Upon this discovery, third

generation aluminum-lithium alloys consisting of around 1 wt% lithium; such as 2050 and 2195 were developed (Table II).

Table II: Compositions of Al-Li alloys 2195 and 2050 (wt%)[2]

Alloys	Li	Cu	Mg	Ag	Zr	Sc	Mn	Zn	Al	Density (ρ/cm^{3})
2195	1.0	4.0	0.4	0.4	0.11	0	0	0	Bal	2.71
2050	1.0	3.6	0.4	0.4	0.11	0	0.35	0.25	Bal	2.70

The increase in Young's modulus and decrease in density results in a synergistic effect on the specific stiffness (E/ρ). Al-Li alloys have better mechanical properties than 7075 Al, and replacing them in metallic aircraft structures offers a potential of up to 6% weight reduction which makes them attractive for aerospace applications.[6] The downside of Al-Li alloys is their high cost to manufacture. Lithium reacts with oxygen and nitrogen in dry air forming oxides that must be removed before any further processing may take place. Oxide removal is done by specialized casting equipment that makes the overall manufacturing cost of aluminum-lithium alloys more expensive.[5]

1.2.4 Corrosion

Corrosion is defined as an electrochemical reaction between a material and its environment that causes physical deterioration to the material as well as its properties. There are many forms of corrosion, which tend to be most prevalent in metals. There are four main requirements (Figure 3) for a corrosion cell. These parts include an anode, cathode, ionic current path, and electron path.

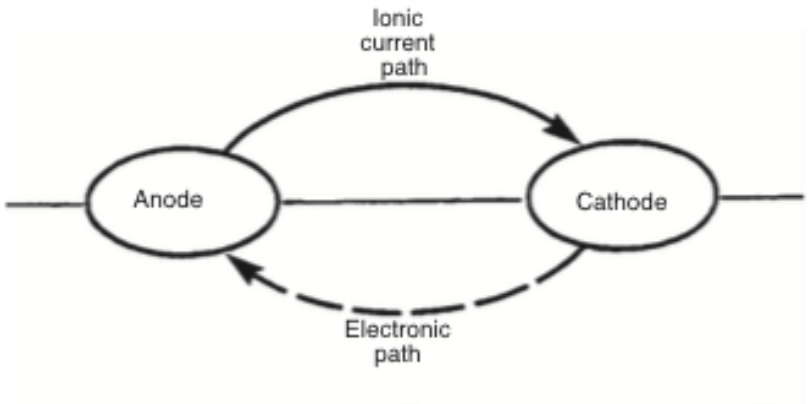

Figure 3: Four main requirements of a corrosion cell with visible current direction. [6]

Corrosion reactions are an exchange of electrons. In an electrochemical cell, oxidation reactions are occurring at the anode, generating electrons and causing metal loss. The metal is breaking down into the form of positively charged ions and travels through the electrolyte forming a passive film on the cathode. The electrons that are produced at the anode are traveling along the electronic path towards the cathode where they are consumed by the reduction reaction occurring at the surface. These reactions accelerate the corrosion of the anode, but inhibit corrosion at the cathode.[6]

1.2.5 Galvanic Corrosion

Galvanic corrosion is a type of corrosion that occurs when a metal comes into contact with another conducting material in a corrosive medium. In order for this to happen, there must be a common electrolyte, a common electrical path, and two or more materials that have a different surface potential. When this occurs, a galvanic current flows from one metal to the other, with the amount of corrosion being directly proportional to the current flow.[7] This often occurs when dissimilar metals are brought into electrical contact with one another in the presence an electrolyte, forming a galvanic couple. The direction of the galvanic current is determined by the activeness of each of the metals in the galvanic couple. When the galvanic couple is formed, one of the metals will act as the anode, corroding at a higher rate than it would on its own, while the other metal would become the cathode, and would be protected in the sense that it would corrode at a rate slower than it would by itself. In aircraft design, dissimilar metals are often joined and the potential of the metals to galvanically corrode is important to take into consideration.

1.2.6 Galvanic Series

Although there is more than one factor that affects galvanic corrosion, the driving force for it to occur is the potential difference between the different metals.[8] A galvanic series is a practical way to predict the potential between two metals for galvanic corrosion to occur because it displays the difference in electrochemical potential between a variety of metals (Figure 4).

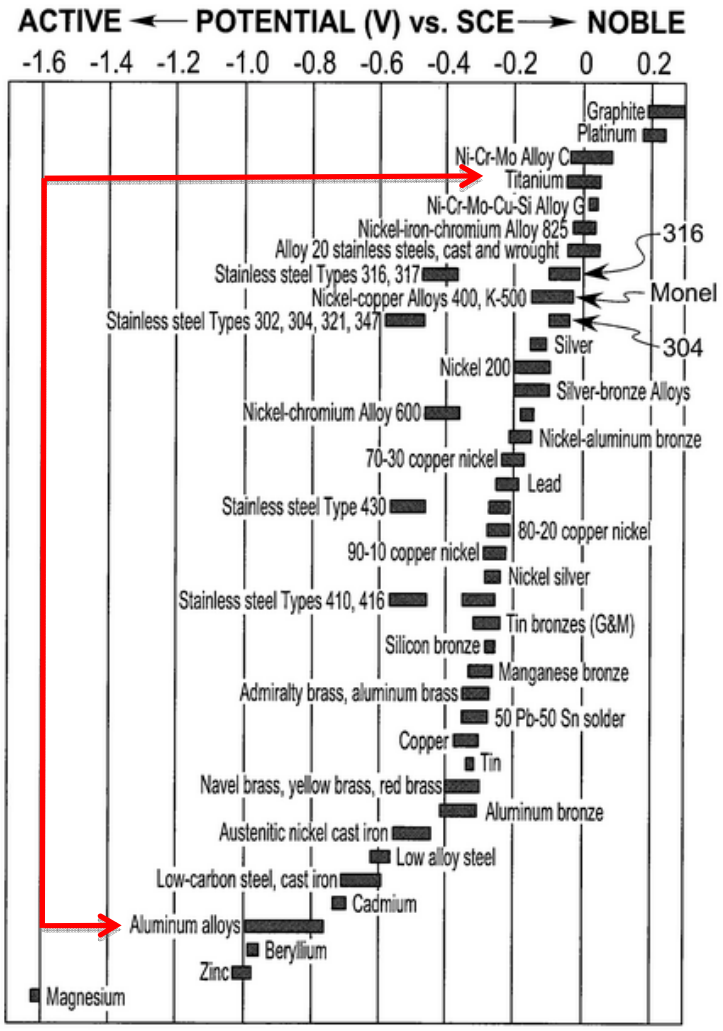

Figure 4: The galvanic series in a 3.5% NaCl solution representing seawater can be used to visualize the difference in electrochemical potential between aluminum and titanium alloys. A calomel reference electrode was used.[9]

Aluminum alloys tend to have negative electrochemical potentials, making them more active, and more likely to corrode when joined with other metals. Titanium on the other hand, is more

noble, and when in contact with other metals, usually behaves as the cathode and corrodes at a significantly slower rate.

1.2.7 Marine Environment

Although technological advances and many years of experience have helped decrease the amount of aircraft failures in the last fifty years, corrosion resistance is still a pivotal part of the design requirements in fracture critical aircraft components. Airplanes often travel through sea air, a particularly corrosive electrolyte, meaning that the joined dissimilar metals that make up the structure of the aircraft could be susceptible to galvanic corrosion. Sea water contains 3.5% NaCl, which is one of the most corrosive concentrations of salt.[12]

1.3 Testing

1.3.1 Electrochemical Testing

As previously mentioned, we will be investigating the effect of galvanically coupling various aluminum alloys to Ti-6Al-4V and will be able to rank each alloy on their corrosion resistance. A commonly used method to quantify galvanic activity is electrochemical testing. These tests can effectively measure the electrochemical potentials of two alloys, the current between them, and the rate that polarization will occur; while also being a relatively quick and accurate experiment to perform.[11]

As previously mentioned, during galvanic corrosion, oxidation reactions are occurring at the anode while simultaneously a reduction reaction is occurring at the cathode which results in a galvanic current to flow between the two dissimilar metals. The driving force for this corrosion reaction is the difference in electrochemical potential between the cathode and the anode in the corrosion cell, and the reaction rate is equal to the current that flows through the cell. The total resistance of the corrosion cell is equal to the sum of the individual resistances related to the anode, cathode, ionic bridge, and electronic path. These three variables can be related using Ohm's law (V=IR), and electrochemical tests are performed by controlling one or two of these variables to solve for another. The likelihood of detrimental galvanic action can be determined by the difference in electrochemical potentials between two metals in contact with the same electrolyte. These potential values can be quantified by the use of a potentiostat.[12]

A potentiostat is a device that controls the voltage of a circuit to make electrochemical measurements. A standard potentiostat testing setup consists of a working electrode (test specimen), reference electrode (saturated calomel), and counter electrode (graphite). The potentiostat maintains a constant voltage to the test specimen with respect to the reference electrode which is comprised of a metal immersed in an electrolyte that has a known electrochemical potential that does not vary with time. The reference electrode acts as a baseline from which to measure the potential of the test specimen. The basic component of a potentiostat is a voltage feedback operational amplifier. The input of the operational amplifier applies the necessary current to maintain the voltage difference between the working and reference electrodes referred to as the control voltage (V_c) while the output is connected to the counter electrode to complete the circuit. Essentially, throughout the test the potentiostat applies the necessary cell current to the circuit in order to maintain V_c between the reference and working electrodes. This allows the device to determine V_{cell} which is the applied voltage in order to maintain V_c and will constantly be changing in order to maintain the fixed value of V_c. The current required to generate V_{cell} is referred to as the polarization current.[11]

1.3.2 Polarization

The two main types of polarization are concentration and activation. Concentration polarization is controlled by the mass transport of reacting species to the electrode surface or reaction products in the solution, and occurs when the solution becomes saturated which limits the total current. In activation polarization, corrosion is controlled by the driving force at the surface of the reaction which is referred to as the difference in potential values of the anodic and the cathodic regions. Mixed potential theory states that in an electrochemical cell anodic and cathodic current must be equal, so each reaction can be treated separately. Both reactions are plotted on the same graph of potential vs the log of current and can be used to determine the potential (E_{corr}), and current (I_{corr}) of the corrosion cell. These two values can be extrapolated by observing where the anodic and cathodic reactions intersect which is referred to as steady state, which can be seen in Figure 5.

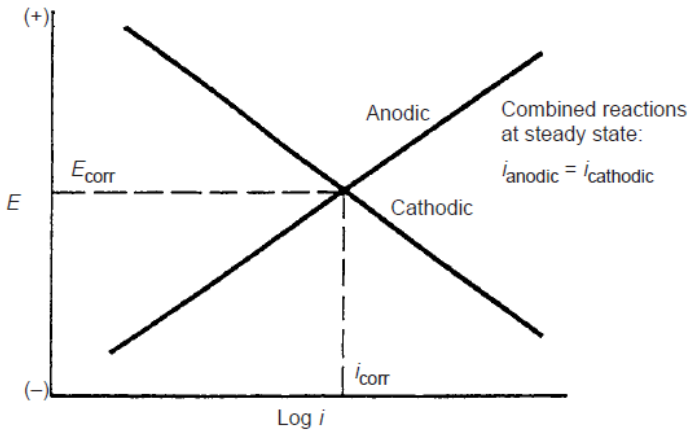

Figure 5: Schematic of potential vs. log of current, and displaying where E_{corr} and I_{corr} can be extrapolated.[11]

A common method to generating this plot is through potentiodynamic polarization, which can be done using a potentiostat.

1.3.3 Potentiodynamic Polarization

Potentiodynamic polarization techniques permit the measurement of polarization behavior by continuously scanning the potential (V_{cell}) while monitoring the current response. To find steady state conditions, which are essential to extrapolating the E_{corr}, the sweep selection rate is important. ASTM Standard G5 specifies a sweep rate of 0.6 V/hr (10mV/min) for many metal-environment conditions. The test begins at a low potential and increases by small steps following the sweep rate making current measurements at each potential reading until it reaches an upper limit. Throughout the process polarization curves for the anodic and cathodic reactions are generated. This current-potential relationship can be used to determine corrosion characteristics of a metal specimen in an aqueous environment.

However, the curves generated are not linear such as the plot shown in Figure 5, but can be seen in Figure 6.

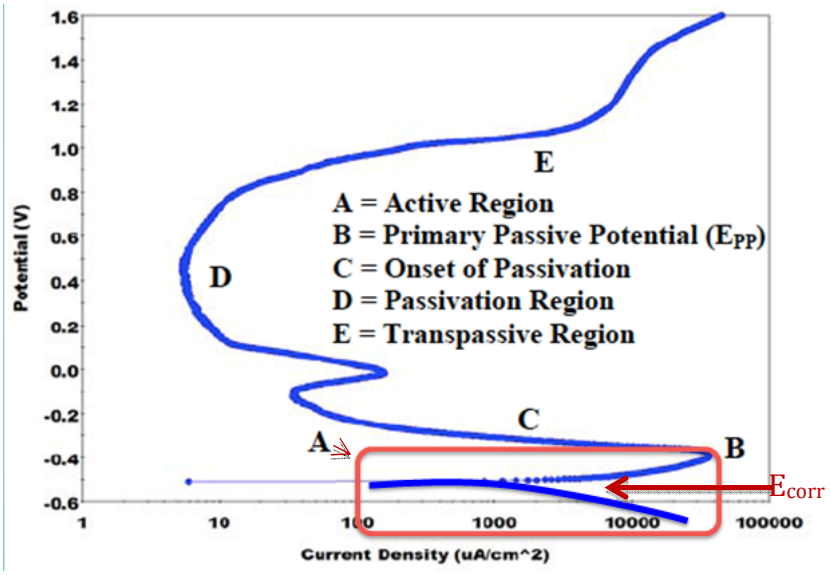

Figure 6: Potentiodynamic anodic polarization plot of 430 stainless steel showing all of the possible regions associated with corrosion behavior of a sample.[13]

Region A of the plot is known as the active region in which the sample is corroding, but at B a critical potential value is reached and the material begins to reach the onset of passivation and the corrosion rate decreases. The corrosion rate is slowing down due to a chemical loss of reactivity to the environment as a passive film is beginning to form inhibiting corrosion. At region C, the formation of the film is causing the current to decrease rapidly while the potential stays around the same. However, at region D the current stays relatively the same while the potential is increasing rapidly due to the full passivation of the sample, but once it reaches region E the passivating film begins to break down known as the transpassive region and the sample will actively corrode for the duration of the test. The boxed region shows the active polarized anodic and cathodic region around the open circuit potential. For the purpose of this project, this region is the most important considering it can be used to determine the electrochemical potential value (E_{corr}). The software will generate Tafel slopes which are linear approximations of the anodic and cathodic regions so an E_{corr} value can be extrapolated.[11]

Potentiodynamic anodic polarization techniques will allow E_{corr} values for the various test alloys to be extrapolated. These determined E_{corr} values will be used to develop a galvanic series which will allow us to predict which aluminum alloy will show the least corrosion when coupled to Ti-6Al-4V.

2. Experimental Procedure

Potentiodynamic polarization tests were performed on each of the alloys using a Princeton Applied Research Parstat 2273 and K0047 Corrosion Cell, following ASTM Standard G5.[14] The alloys being tested were provided by Weber Metals and machined to the dimensions specified in the user manual for the K0047 Corrosion Cell Kit by Dugandzic Design (San Luis Obispo, CA). Some of the samples were provided in the T852 condition and they were artificially aged at 155°C for 20 hours. Each sample that was tested was machined into cylindrical specimen ½" long, 3/8" in diameter drilled to a depth of ¼" and tapped to accept a 3-48 thread. These specific dimensions can be seen in Figure 7.

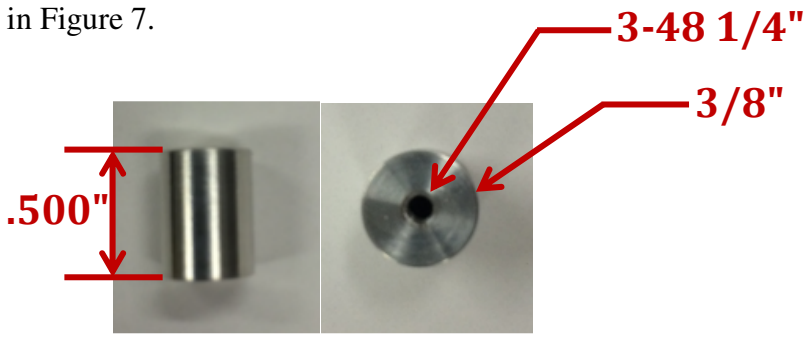

Figure 7: Sample dimensions in inches.

2.1 Safety

Safety was of the utmost importance throughout the duration of this project. Protective eyewear, close-toed shoes, and long pants were worn at all times when in the lab. Rubber gloves were worn when handling the acetone during the degreasing process and degreasing was performed under a fume hood.

2.2 Sample and Corrosion Cell Cleaning

Each sample was fully submerged in a beaker of acetone, which was then placed in an ultrasonic bath filled with water and agitated for five minutes, in accordance to ASTM Standard G1.[15] The sample was then removed from the acetone beaker and rinsed thoroughly using deionized water, before air-drying. Following ASTM Standard G5, the samples were then wet ground on all surfaces using 240-grit SiC paper, and then wet polished using 600-grit SiC paper to remove the previous scratches and generate a reproducible surface finish.

The entire corrosion cell, including the corrosion flask, specimen holder, and both counter electrode holders were rinsed with ethanol and then distilled water before being left to air dry before each test was performed.

2.3 Preparing the Electrolyte

The electrolyte chosen for this experiment was a 3.5% NaCl solution, approximating seawater. Since these alloys will be used to make aircraft that travel though sea air, this electrolyte represents the most extreme corrosive environment that the material would be exposed to in its lifetime. The electrolyte was made by adding 34 +/- 0.001 g of Morton's iodized salt to 920 mL of distilled water and stirring thoroughly until a homogenous solution was obtained.

2.4 Corrosion Cell Setup

Once the corrosion cell and sample were properly cleaned and the electrolyte was prepared, the corrosion cell was set up following the instructions in the Princeton Applied Research Operating Manual. The fully assembled corrosion cell with labeled parts can be seen in Figure 8. The sample was screwed onto the specimen holder and a Teflon part protected the sample from touching the rod holder.

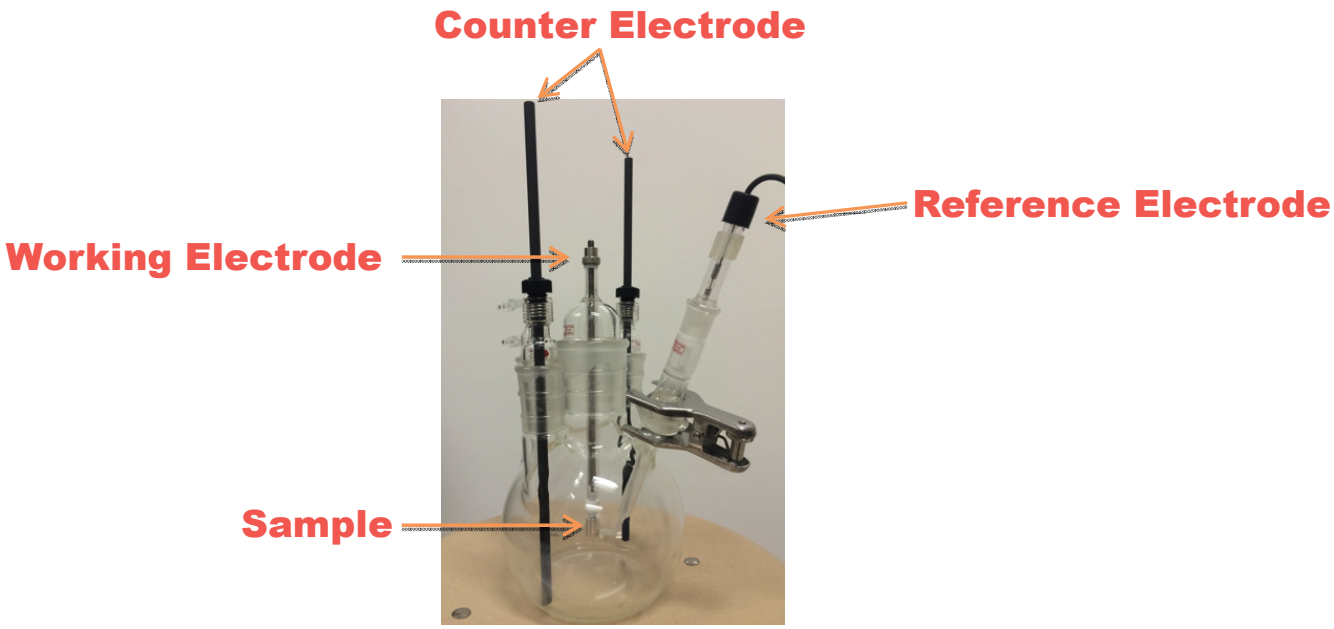

Figure 8: Fully assembled corrosion cell including the working electrode, reference electrode, counter electrodes, and the corrosion sample.

The corrosion cell consisted of three parts: the working, reference, and counter electrodes. The working electrode acted as the anode in the corrosion cell and held the sample. The counter electrode acted as the cathode in the corrosion cell, and consisted of graphite rods due to their high electrochemical potential (Figure 4). The main purpose of the graphite rods was to accelerate corrosion of the sample while also remaining inert to prevent contamination of the solution from its ions. The reference electrode, a saturated calomel electrode for these experiments, consisted of a metal immersed in an electrolyte with a known potential that would not vary with time and acts a baseline to make measurements of the potential at the working electrode. Each of these electrodes was connected to the potentiostat with the addition of a sense lead connected in series with the working electrode. A resistor was placed between the sense and working electrode to prevent noise in the data. The purpose of the sense lead was to act as a secondary source to measure the voltage at the sample.

2.5 Potentiodynamic Testing

After the corrosion cell was set up, the salt solution was agitated and then left for 30 minutes to reach equilibrium. The PowerCORR software required the surface area of the sample, as well as the equivalent weight of each alloy tested. The equivalent weight of each alloy was calculated by dividing the atomic weight of each alloying element by its most stable charge, and then multiplying it by its corresponding weight percentage in the alloy. The obtained values for each alloying element were then added together yielding the overall equivalent weight of the alloy. The surface area of each sample was constant at 4.041 cm^2, and the equivalent weight for each alloy can be seen in Table III.

Table III: Equivalent Weights of Each Alloy Tested

Alloy	Equivalent Weight (g)
7075	10.783
2195	10.355
2050	10.291
Ti-6Al-4V	11.999

Once the corrosion cell had been connected to the potentiostat, a measurement of the open circuit potential was taken to act as a point of reference for the range tested. For each test, a range of -250 mV to the open circuit potential to 1600 mV above was scanned at a rate of 0.1660 mV/sec. The test was left to run until a curve with the appropriate shape of the active region was formed which can be seen in Figure 9.

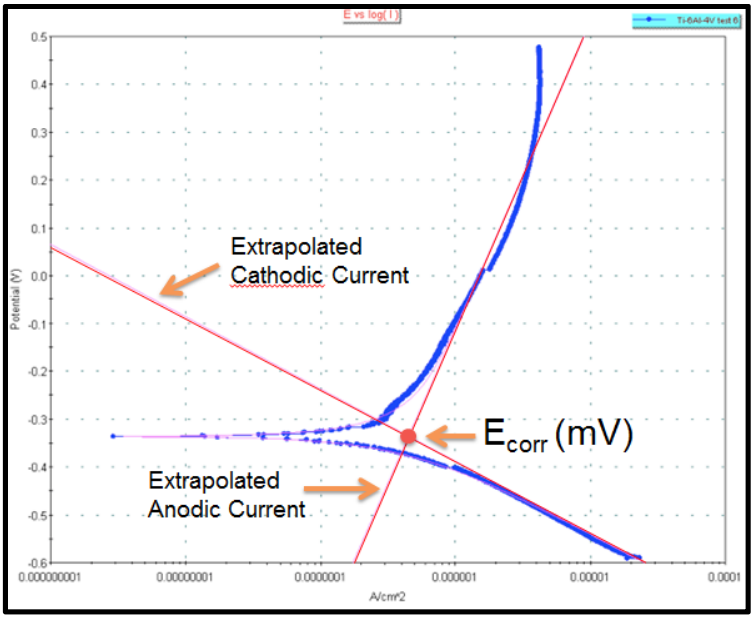

Figure 9: Polarization curve of a Ti-6Al-V sample. The point at which the linear approximations intersect an electrochemical potential value (E_{Corr}) can be extrapolated.

For each of the five alloys tested, nine polarization curves were recorded and an electrochemical potential value was extrapolated.

2.6 Statistical Analysis of Corrosion Data

JMP software was used to statistically analyze the electrochemical potential values obtained during potentiodynamic testing. Specifically, the data was organized in boxplots by alloy in order to schematically show the potential difference between Ti-6Al-4V and each of the aluminum alloys. Since each of the aluminum-lithium alloys had similar mean potential values, analysis of variance was performed in order to determine if the means were statistically different from one another. Specifically, three separate t-tests were run, comparing the mean potential values of each of the aluminum-lithium alloys to each other. Final recommendations for further testing were made from statistical analysis of the corrosion data.

3. Experimental Results

3.1 Potentiodynamic Polarization

A polarization curve was generated from each potentiodynamic polarization test. The shape of each curve was similar, showing an actively corroding region. A polarization curve for 2050 T3 can be seen in Figure 10.

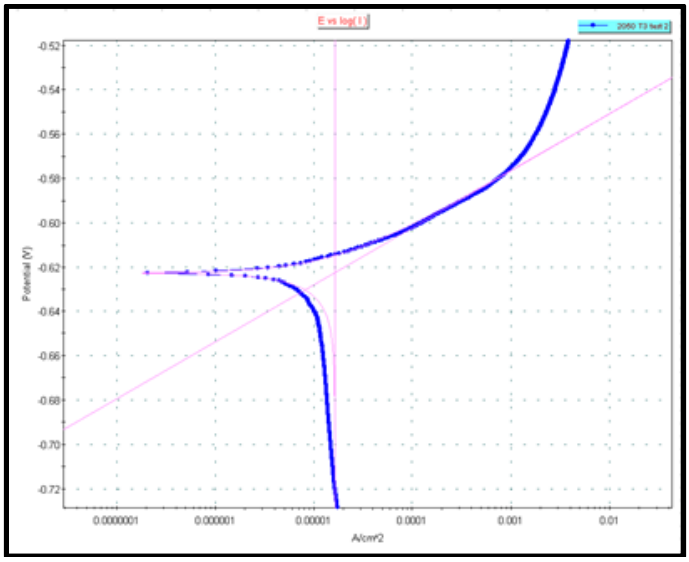

Figure 10: Potentiodynamic polarization curve for the 2050-T3 condition from one of the nine tests.

The 2050-T3 curve has a similar shape to the Ti-6Al-4V curve shown in Figure 9, but the anodic and cathodic regions intersect at a potential value much lower than Ti-6Al-4V, which was expected. The curve for the 2050-T852 condition is almost identical to the T3 condition (Figure 11).

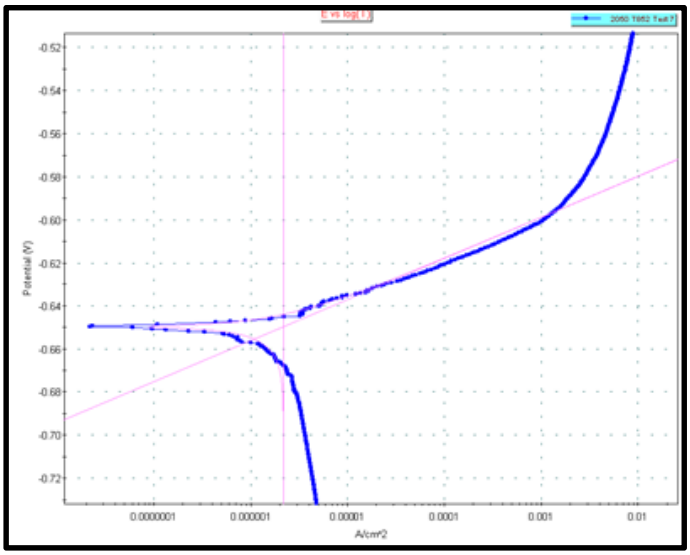

Figure 11: Potentiodynamic polarization curve for the 2050-T852 condition from one of the nine tests.

The only difference in the curves between the T852 and T3 conditions is that the extrapolated electrochemical potential value is slightly lower in the T852 condition, but the shapes of the anodic and cathodic regions are almost identical. Small differences can be seen in the 2195 plot (Figure 12).

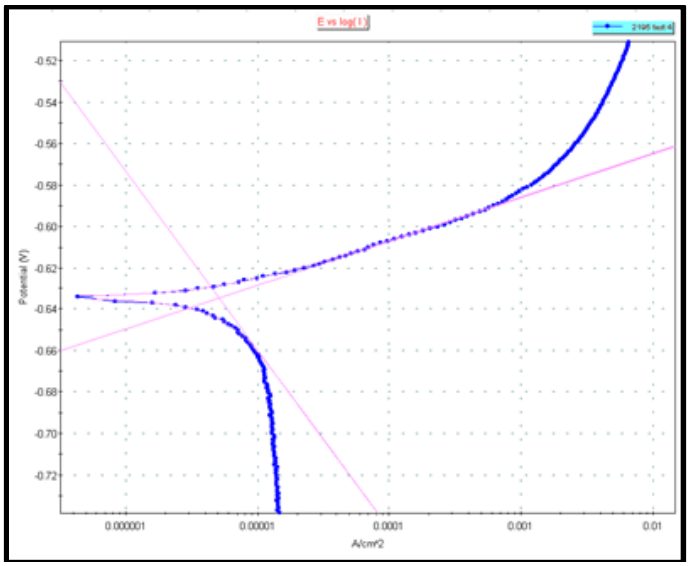

Figure 12: Potentiodynamic polarization curve for 2195 from one of the nine tests.

The plot for 2195 showed an active region, which was constant throughout all alloys tested, but the gap between the anodic and cathodic regions was larger than the 2050-T3 and 2050-T852

condition. This allowed the software to make more accurate linear approximations of the anodic and cathodic curves than in the 2050 plots. There was more difficulty in fitting the Tafel slope for 7075 (Figure 13).

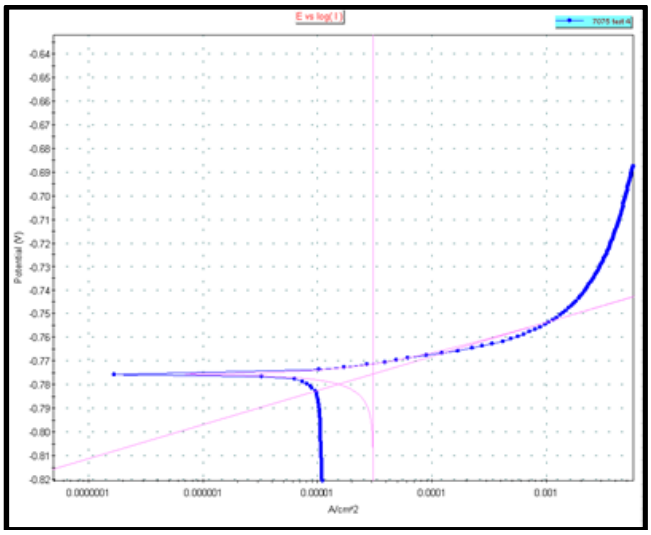

Figure 13: Potentiodynamic polarization curve for 7075 from one of the nine tests. The linear approximations of the anodic and cathodic regions are not as accurate as the other alloys tested.

The 7075 samples had the same general shape as the other alloys tested; however, there was a small gap between the anodic and cathodic regions, which made the linear approximations of these regions to be inaccurate. It can be noted that even though the Tafel slopes were off, the 7075 showed the least amount of variance between the alloys tested.

The polarization curves yielded the electrochemical potential of each of the alloys that were tested and the corrosion potential is shown in Table IV.

Table IV: Electrochemical Potential Values from Potentiodynamic Testing

Alloy	7075	2195	2050 T3	2050 T852	Ti-6Al-4V
Test Number	(mV)	(mV)	(mV)	(mV)	(mV)
1	-785.581	-658.029	-608.180	-668.644	-283.927
2	-774.550	-645.607	-622.554	-673.866	-332.208
3	-773.754	-641.548	-601.769	-658.983	-318.540
4	-775.513	-634.623	-632.192	-645.621	-331.820
5	-765.946	-622.761	-638.774	-629.216	-375.600
6	-766.058	-621.865	-599.148	-654.093	-335.657
7	-770.033	-639.622	-607.845	-649.965	-377.184
8	-771.647	-608.153	-611.020	-649.157	-339.133
9	-765.266	-627.546	-602.641	-634.934	-299.192
Average	-772.040	-633.310	-613.790	-651.610	-332.580
Standard Deviation	6.3997	14.9166	14.1303	14.4490	30.7660
Range	20.315	49.876	39.626	44.650	93.257

Ti-6Al-4V showed the most positive corrosion potential out of all the alloys tested, making it the most noble with an average electrochemical potential of -332.580 mV. 7075 Al was the most active alloy tested, with an average potential value of -772.040 mV. Each of the three aluminum-lithium alloys tested had more positive potential values than 7075 making them less active than the current industry standard material. Other than 7075, each alloy tested exhibited a significant amount of scatter between each test, but Ti-6Al-4V showed the most. This high amount of scatter in each population caused a high standard deviation value, but it is typical to observe this amount of variance in corrosion testing.

The electrochemical potential difference between each of the aluminum alloys and Ti-6Al-4V was taken, in order to show which alloy would be the least susceptible to galvanic corrosion when coupled with Ti-6Al-4V. This difference in mean potential values can be seen in Table V.

Table V: Average Potential Difference Between Aluminum Alloys and Ti-6Al-4V

Alloy	Potential Difference (mV)
2050-T3	281.21
2195-T852	300.73
2050-T852	319.03
7075-T7352	439.46

Each of the three aluminum-lithium alloys had a lower potential difference than 7075 aluminum. 2050-T852 had the greatest potential difference out of each of the aluminum-lithium alloys and still out performed 7075 by over 100 mV. Also, it is worth noting that the naturally aged 2050-T3 had a lower potential difference than the artificially aged 2050-T852.

3.2 Statistical Analysis

There was significant variation between the potential values determined by each test for the given alloys. The variation can be seen schematically by the statistical boxplots shown in Figure 14.

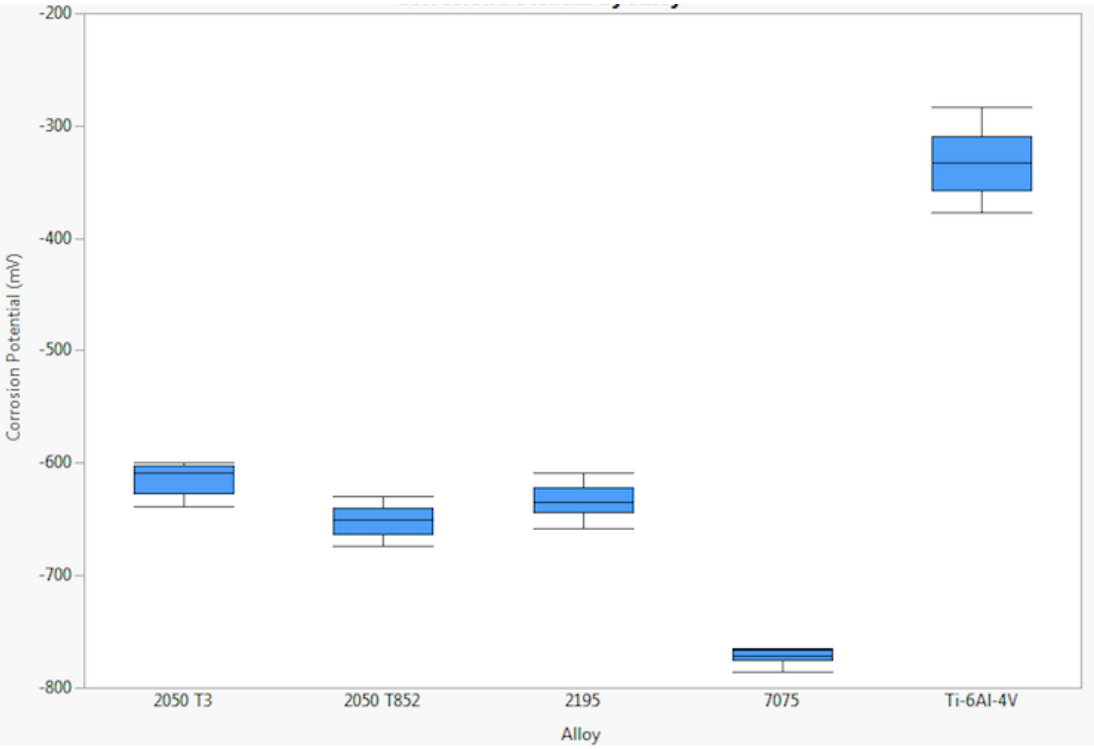

Figure 14: Boxplots of the variation and mean potential values of each of the alloys tested.

Each boxplot represents the range of corrosion testing data for that particular alloy. The area in blue on the boxplots represents 50% of the data and the lines above and below the boxes each represent 25%. Since the Ti-6Al-4V has more variance than any of the other alloys, it has a larger amount of blue space. There is a high amount of variance in all of the alloys except for 7075, but this is common for corrosion data.

Since the average potential values for each of the aluminum-lithium alloys were relatively close to one another, analysis of variance was performed in order to determine if the means were statically different from one another. In doing so, three separate t-tests were performed comparing the means of each aluminum-lithium alloy to one another. The P-values obtained from each of these t-tests were less than 0.05 meaning that with 95% confidence, it can be said that the mean potential values of 2195, 2050-T3, and 2050-T852 are statistically different from one another.

3.3 Visual Inspection

In addition to the polarization curves, a visual inspection was done after each test to see if there was a noticeable amount of corrosion. The observed amount of corrosion for each alloy can be seen in Figure 15.

Figure 15: The visual corrosion on the samples at the end of each test was observed. It can be noted that all of the aluminum-lithium alloys had about the same amount of visible corrosion as the 2050-T852 samples.

The Ti-6Al-4V sample showed little to no corrosion, which was expected due to its high electrochemical potential. The 7075 samples showed significantly more corrosion product than

all of the other alloys tested. The aluminum-lithium alloys showed signs of corrosion, but still less than 7075.

4. Discussion

4.1 Influence of T3 and T852 Aging Conditions on Corrosion Potential

The corrosion behavior of the 2050 Al-Li alloy has a lot to do with the precipitation of the main strengthening phase known as T_1 (Al_2CuLi). The distribution of the precipitates in each condition can be seen in Figure 16.

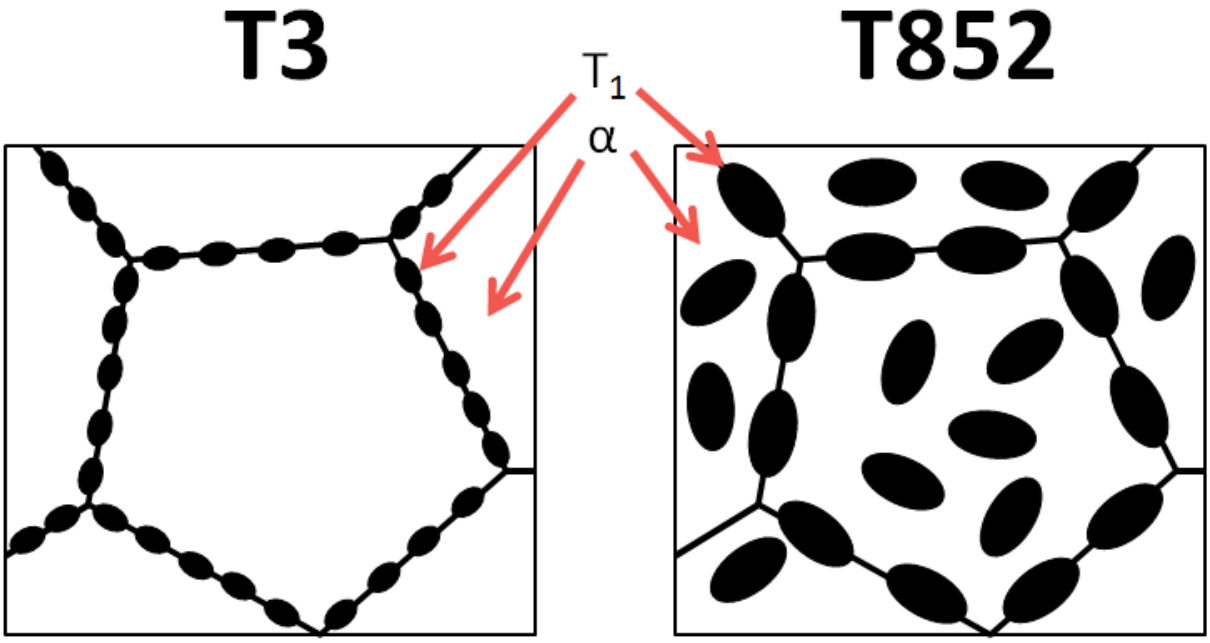

Figure 16: Pictorial representation of the nucleation of the T_1 precipitates in the T3 and T852 condition.

In the T3 condition the T_1 precipitates stay restricted to the grain boundaries, but in the T852 condition, they grow a little in size and distribute themselves within the grains. To form these precipitates the matrix has to give up copper and lithium, which causes the regions adjacent to the precipitates to be a more pure form of aluminum. The lack of copper at these locations cause the electrochemical potential of the matrix to be different than that of the precipitate. This causes a microgalvanic couple to form between these copper depleted regions and the precipitates. At the beginning of exposure to a NaCl solution, the T_1 precipitate is anodic to the matrix, but after

exposure, this effect is reversed and it becomes cathodic to the matrix, which can be seen in Figure 17.

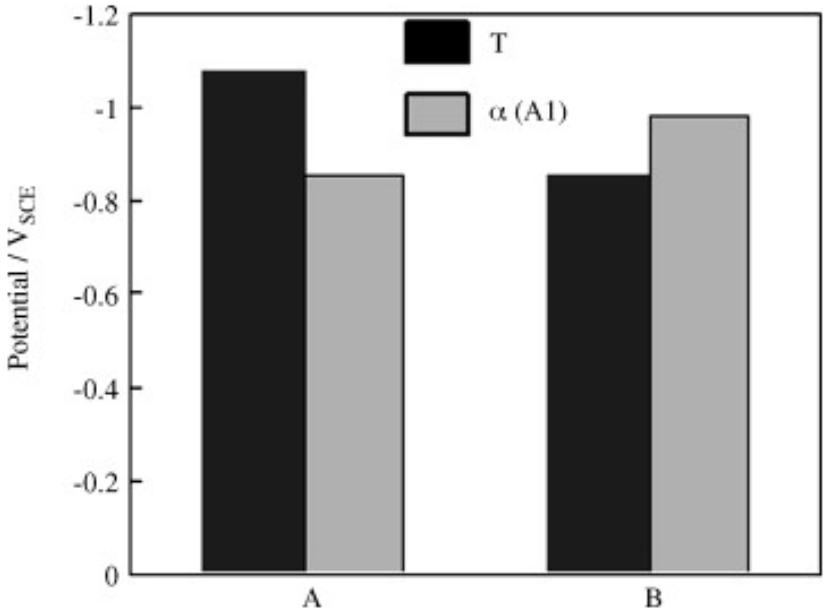

Figure 17: The open circuit potentials of T_1 to the matrix α-Al. A was taken at the beginning of exposure and B was taken after coupling for 10 days.[16]

As a result of this potential shift, the corroded T_1 precipitates became cathodic to the alloy base leading to the anodic dissolution and corrosion of the matrix at the regions directly adjacent to the precipitates. In the T3 condition the T_1 precipitates are restricted to the grain boundaries and exposure to the NaCl solution causes the grain boundaries to dissolve giving the alloy a high susceptibility to intergranular corrosion. In the T852 condition, the distribution of the precipitates causes the alloy to have a susceptibility to pitting as well as intergranular corrosion; however, the artificial aging treatment causes the corrosion that occurs to be less detrimental to the mechanical properties, which can be seen in Figure 18.

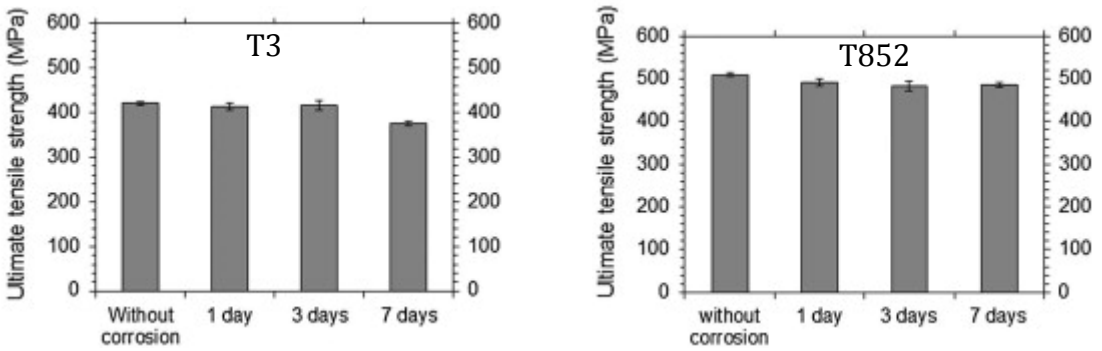

Figure 18: After 7 days of corrosion the tensile strength showed a 10% decrease in the T3 samples, but a 4% decrease in the T852 samples. [17]

It was determined that the depth of intergranular corrosion of the two samples was different, and based on the tensile tests the corrosion damage in the T852 samples was less detrimental to the mechanical properties.[12]

In the T3 samples the T_1 precipitates existed primarily at the grain boundaries and the results showed that the depth affected by intergranular corrosion was larger. As the samples were aged at low temperatures, copper from the matrix was being redistributed to form many small T_1 precipitates throughout the grains and grain boundaries.[12] This phenomena can be seen in Figure 19.

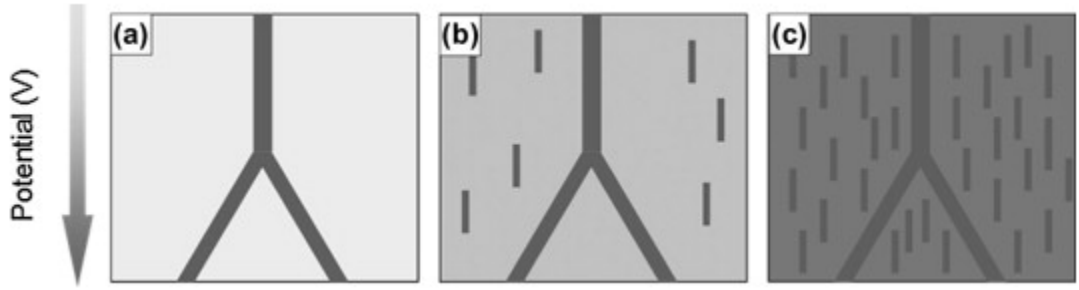

Figure 19: Schematic representation of the electrochemical behavior at the microstructural scale for: (a) T3 samples (b) t_1 aged samples at 155 °C with $t_1 < 9$ h, and (c) t_2 aged samples at 155 °C with $t_2 > 9$ h.[12]

Depleting the copper from the matrix would lower its electrochemical potential, and would reduce the difference in potentials between the matrix and T_1 precipitates. This would reduce the micro galvanic coupling effect because the T_1 particles would be distributed throughout the grains and grain boundaries reducing the alloy's susceptibility to intergranular corrosion.

Artificial aging reduces the susceptibility of intergranular corrosion, but lowers the overall potential of the alloy, which explains why the 2050 T3 samples showed a more positive potential value than the 2050 T852.

4.2 Sources of Variance in Corrosion Data

When viewing the data it is clear that there was some scatter between the populations of each alloy tested (Figure 14). In general, corrosion testing shows a large amount of scatter between tests. Precautions were taken to ensure a repeatable procedure to minimize the scatter; however, some factors could not be controlled.

When preparing the sample prior to every test it was initially degreased in a beaker of acetone and placed into an ultrasonic bath. It was placed in the bath for 5 minutes in each test, but sometimes it was left to sit in the acetone at various times while the rest of the equipment was being prepared. The difference between soak times in the acetone could have lead to variability in the cleanliness of the surface. Variability in the surface also had to do with the fact that the samples were hand ground to achieve a surface finish, but it was impossible to reproduce an exact surface finish between trials.

Another source of scatter in the data was caused from the inhomogeneity of the structure of all the samples. The heat treatments provided to each alloy were constant throughout the group; however, due to impurities entering the crystal lattice the exact structure was not homogeneous throughout each sample. Also, the precipitates would not form in the same place in the matrix in each sample, and this high concentration of certain alloying elements in different areas could result in a higher level of localized corrosion, which could be a cause for scatter in the data. It was also not known if the forging direction of each sample was the same, and it was impossible to ensure that the grain flow and orientation would be uniform throughout each sample.

5. Conclusions

1. The electrochemical potential difference values from Ti-6Al-4V were found to be 281.21 mV for 2050-T3, 300.72 mV for 2195-T852, 319.02 mV for 2050-T852, and 439.45 mV for 7075-T7352.
2. Based on the potential difference values it was concluded that all of the aluminum-lithium alloys would show less galvanic corrosion than 7075.
3. The T3 (naturally aged condition) would show less galvanic corrosion than the T852 (artificially aged for 20 hours at 155°C).

6. References

1. "ENGINEERING STUDY MATERIALS." *: Finishing Operations / Powder Metallurgy / Applications*. N.p., n.d. Web. 4 Jan. 2015.

2. Prasad, N. Eswara, and Amol A. Gokhale. "Aerostructural Design and Its Application to Aluminum-Lithium Alloys." *Aluminum-lithium Alloys: Processing, Properties, and Applications*. Oxford: Elsevier, 2014. Print.

3 ."Alcoa North American Rolled Products -- 7075 Aluminum Alloy Plate and Sheet." *Alcoa North American Rolled Products -- 7075 Aluminum Alloy Plate and Sheet*. N.p., n.d. Web. 29 Nov. 2014.

4. Proton, Vincent, Joël Alexis, Eric Andrieu, Jérôme Delfosse, Alexis Deschamps, Frédéric De Geuser, Marie-Christine Lafont, and Christine Blanc. "The Influence of Artificial Ageing on the Corrosion Behaviour of a 2050 Aluminium–copper–lithium Alloy." *Corrosion Science* 80 (2014): 494-502. *Sciencedirect*. Web. 21 Nov. 2014.

5. Prasad, N. Eswara, and Amol A. Gokhale. "Historical Development and Present Status of Aluminum-Lithium Alloys." *Aluminum-lithium Alloys: Processing, Properties, and Applications*. Oxford: Elsevier, 2014. Print.

6. Davis, J.R. *Corrosion: Understanding The Basics* Materials Park: ASM International, 2000. 24-25. Print.

7. Revie, R. Winston, and Herbert Henry Uhlig. *Uhlig's Corrosion Handbook*. Hoboken, NJ: Wiley, 2011. Print.

8. "Galvanic Corrosion." *Galvanic Corrosion*. NACE International, n.d. Web. 29 Nov. 2014.

9. "Patent US20080128393 - Chromium-free Welding Consumable." *Google Books*. N.p., n.d. Web. 6 Jan. 2015.

10. S.C. Dexter, Corrosion in Seawater, Corrosion: Environments and Industries, Vol 13C, ASM Handbook, ASM International, 2006, p 27–41.

11. Thompson, N. G., and J. H. Payer. *DC Electrochemical Test Methods*. Houston, TX: NACE International, 1998. Print.

12. Davis, J.R. *Corrosion: Understanding The Basics* Materials Park: ASM International, 2000. 49-95. Print.

13. Princeton Applied Research. “Basics of Corrosion Measurements”. Application Note CORR-1.print
14. "ASTM G5 - 14 Standard Reference Test Method for Making Potentiodynamic Anodic Polarization Measurements." *ASTM G5 - 14 Standard Reference Test Method for Making Potentiodynamic Anodic Polarization Measurements*. N.p., n.d. Web. 12 Dec. 2014.
15. "ASTM G1 - 03(2011) Standard Practice for Preparing, Cleaning, and Evaluating Corrosion Test Specimens." *ASTM G1 - 03(2011) Standard Practice for Preparing, Cleaning, and Evaluating Corrosion Test Specimens*. N.p., n.d. Web. 12 Dec. 2014.
16. Li, J.f., C.x. Li, Z.w. Peng, W.j. Chen, and Z.q. Zheng. "Corrosion Mechanism Associated with T1 and T2 Precipitates of Al–Cu–Li Alloys in NaCl Solution." *Journal of Alloys and Compounds* 460 (2008): 688-93. *Sciencedirect*. Web. 21 Nov. 2014.
17. Proton, Vincent, Joël Alexis, Eric Andrieu, Jérôme Delfosse, Alexis Deschamps, Frédéric De Geuser, Marie-Christine Lafont, and Christine Blanc. "The Influence of Artificial Ageing on the Corrosion Behaviour of a 2050 Aluminium–copper–lithium Alloy." *Corrosion Science* 80

7. Appendix

7075 Polarization Curves

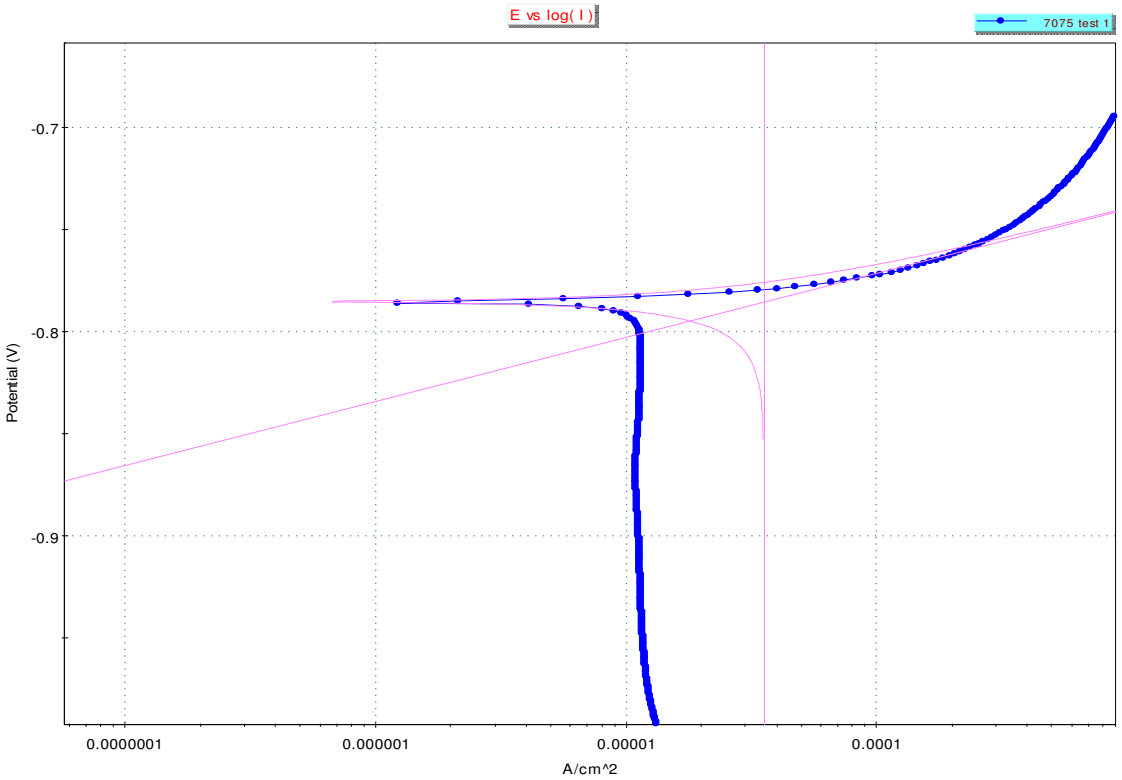

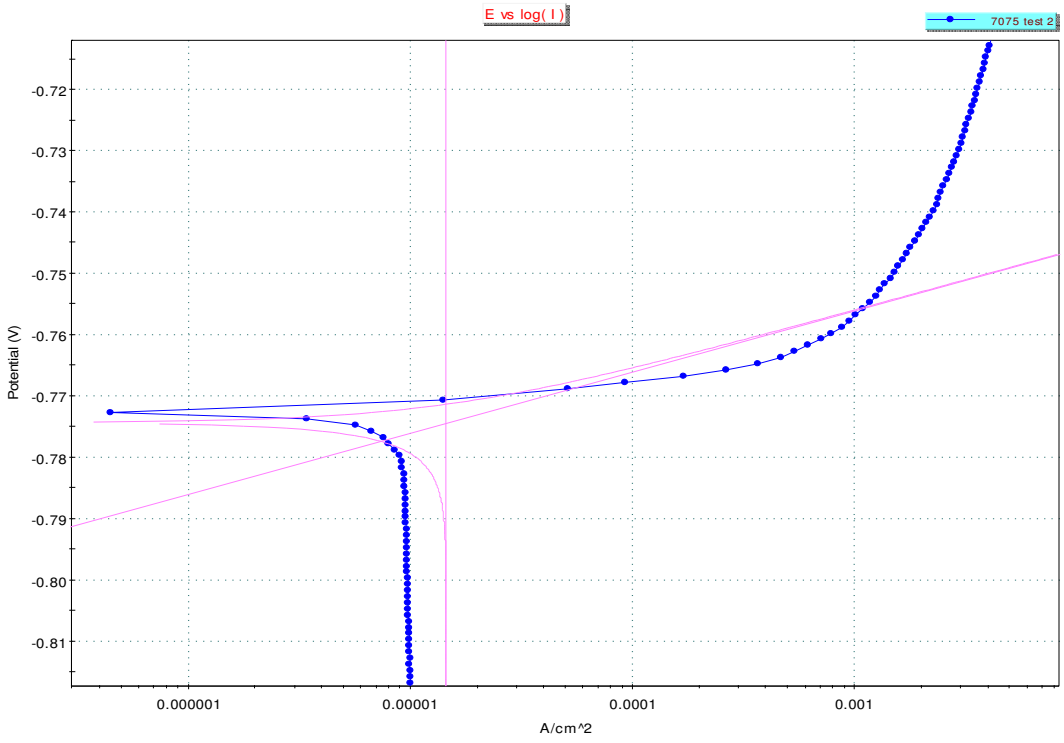

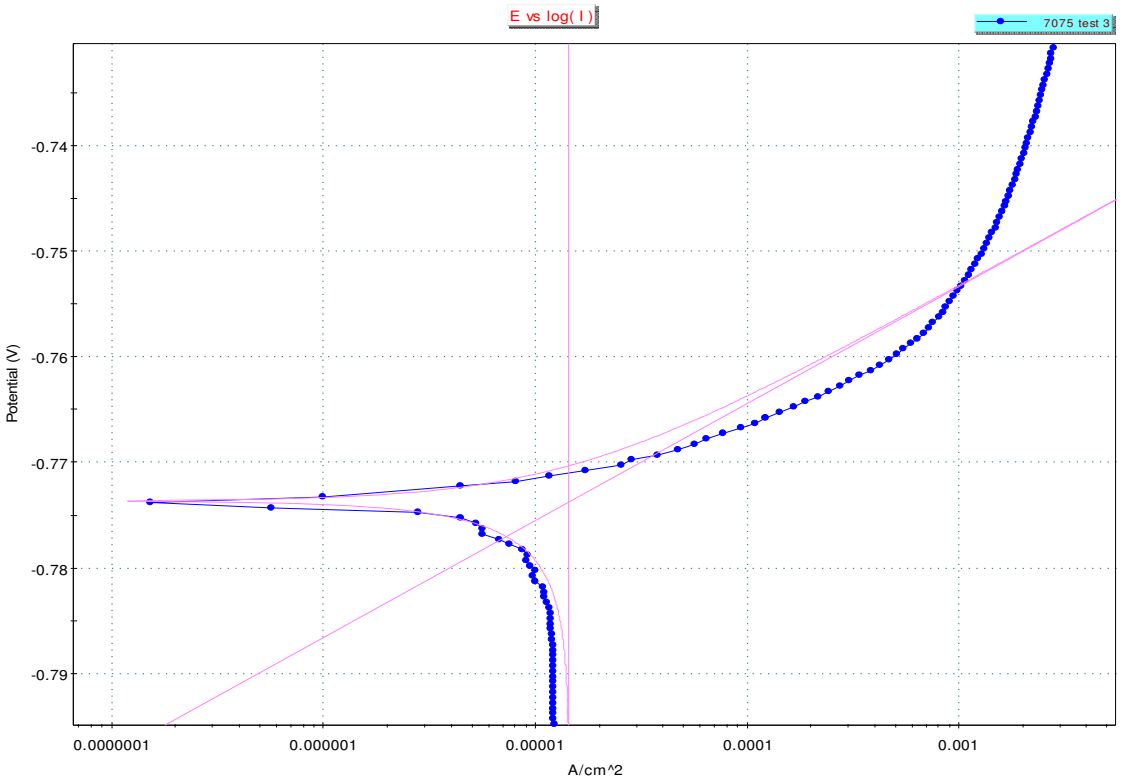
E vs log(I)
7075 test 3
-0.74
-0.75
-0.76
-0.77
-0.78
-0.79
Potential (V)
0.0000001
0.000001
0.00001
0.0001
0.001
A/cm^2

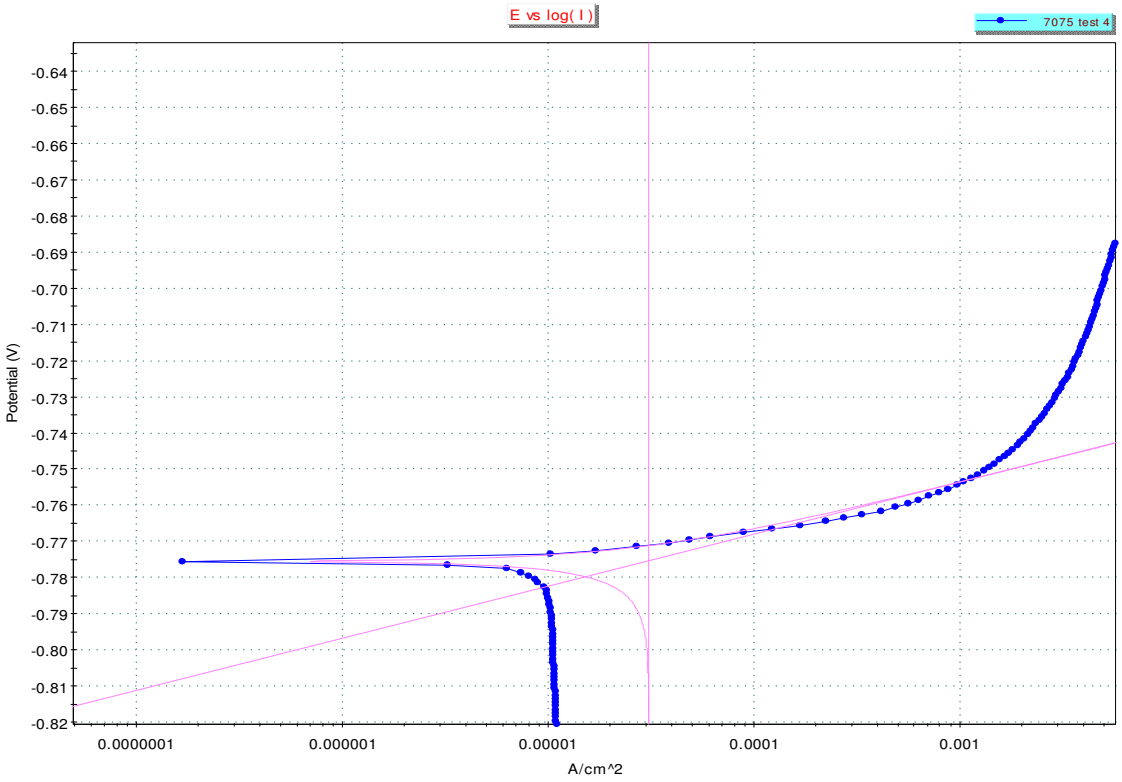
E vs log(I)
7075 test 4
-0.64
-0.65
-0.66
-0.67
-0.68
-0.69
-0.70
-0.71
-0.72
-0.73
-0.74
-0.75
-0.76
-0.77
-0.78
-0.79
-0.80
-0.81
-0.82
Potential (V)
0.0000001
0.000001
0.00001
0.0001
0.001
A/cm^2

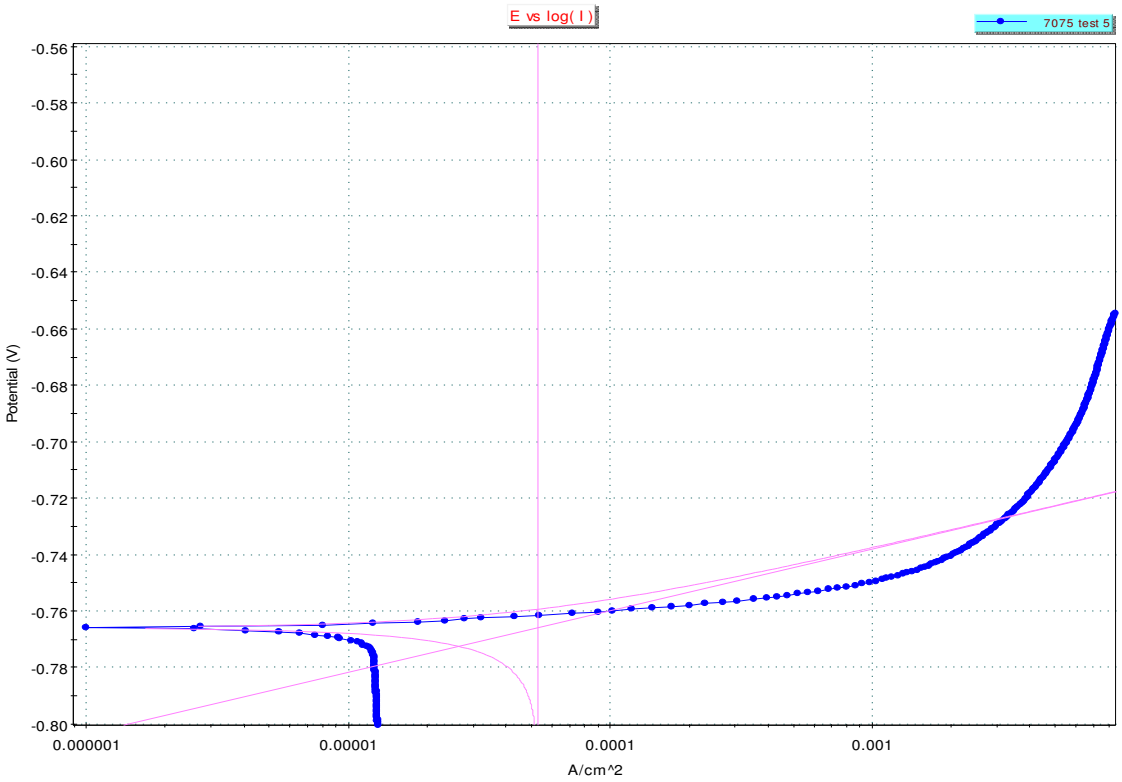
E vs log(I)
7075 test 5
-0.56
-0.58
-0.60
-0.62
-0.64
-0.66
-0.68
-0.70
-0.72
-0.74
-0.76
-0.78
-0.80
Potential (V)
0.000001
0.00001
0.0001
0.001
A/cm^2

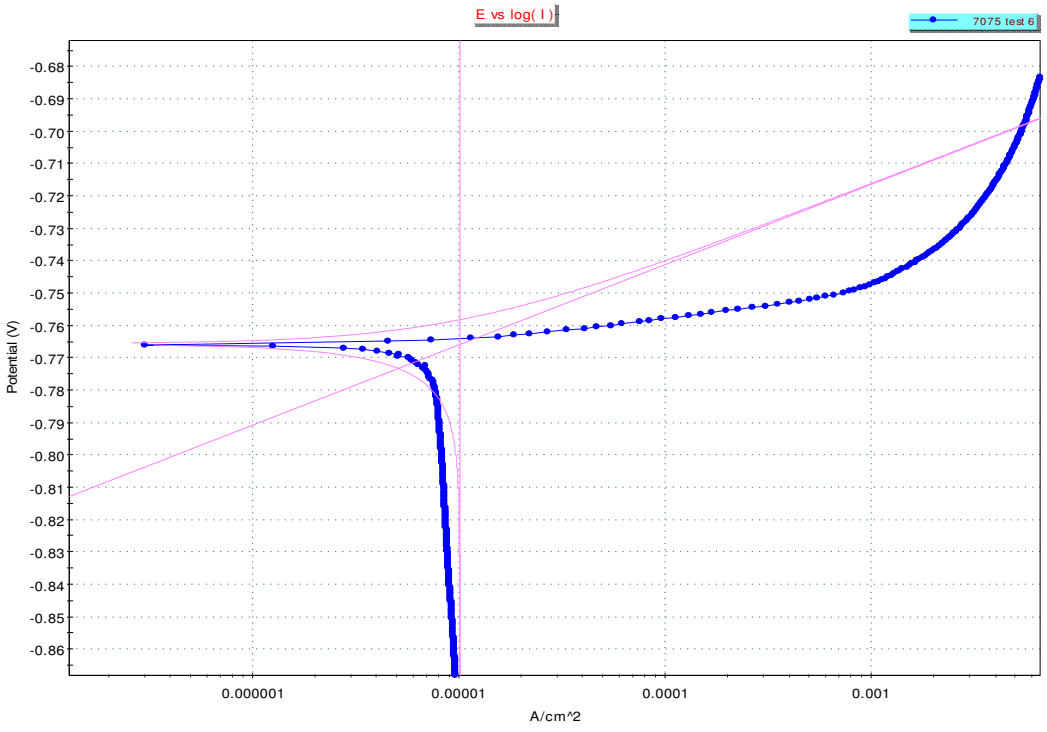
E vs log(I)
7075 test 6
-0.68
-0.69
-0.70
-0.71
-0.72
-0.73
-0.74
-0.75
-0.76
-0.77
-0.78
-0.79
-0.80
-0.81
-0.82
-0.83
-0.84
-0.85
-0.86
Potential (V)
0.000001
0.00001
0.0001
0.001
A/cm^2

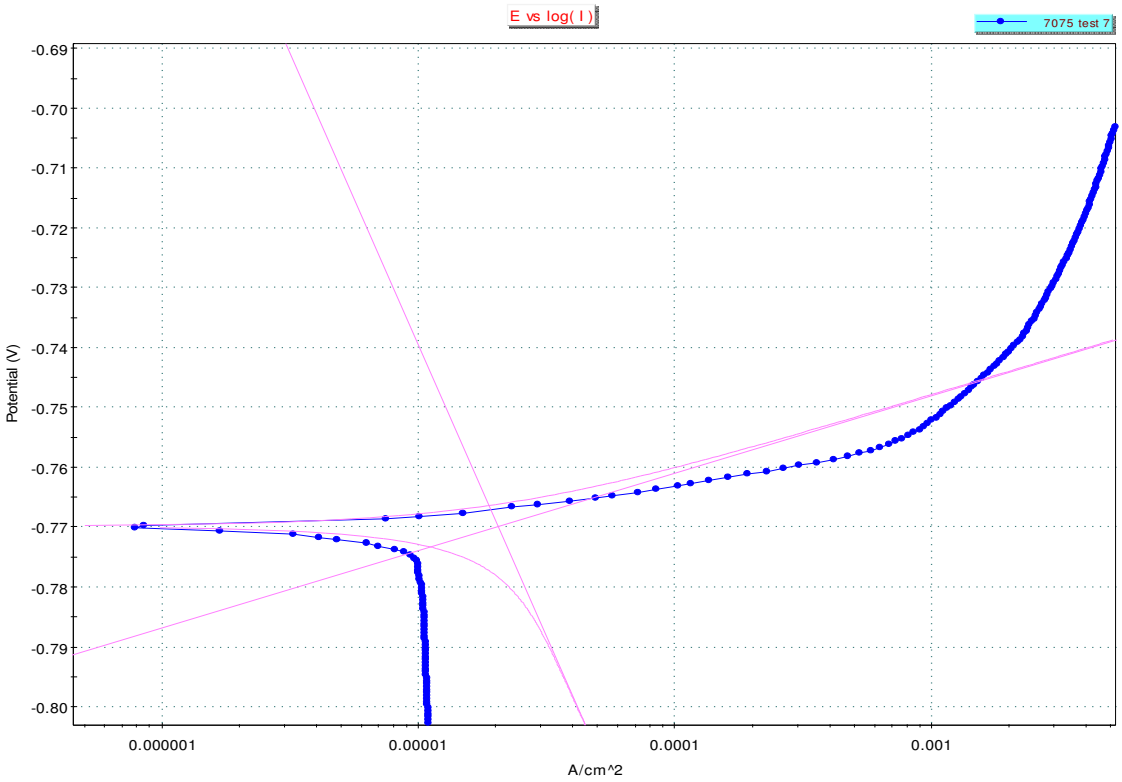
E vs log(I)
7075 test 7
-0.69
-0.70
-0.71
-0.72
-0.73
-0.74
-0.75
-0.76
-0.77
-0.78
-0.79
-0.80
Potential (V)
0.000001
0.00001
0.0001
0.001
A/cm^2

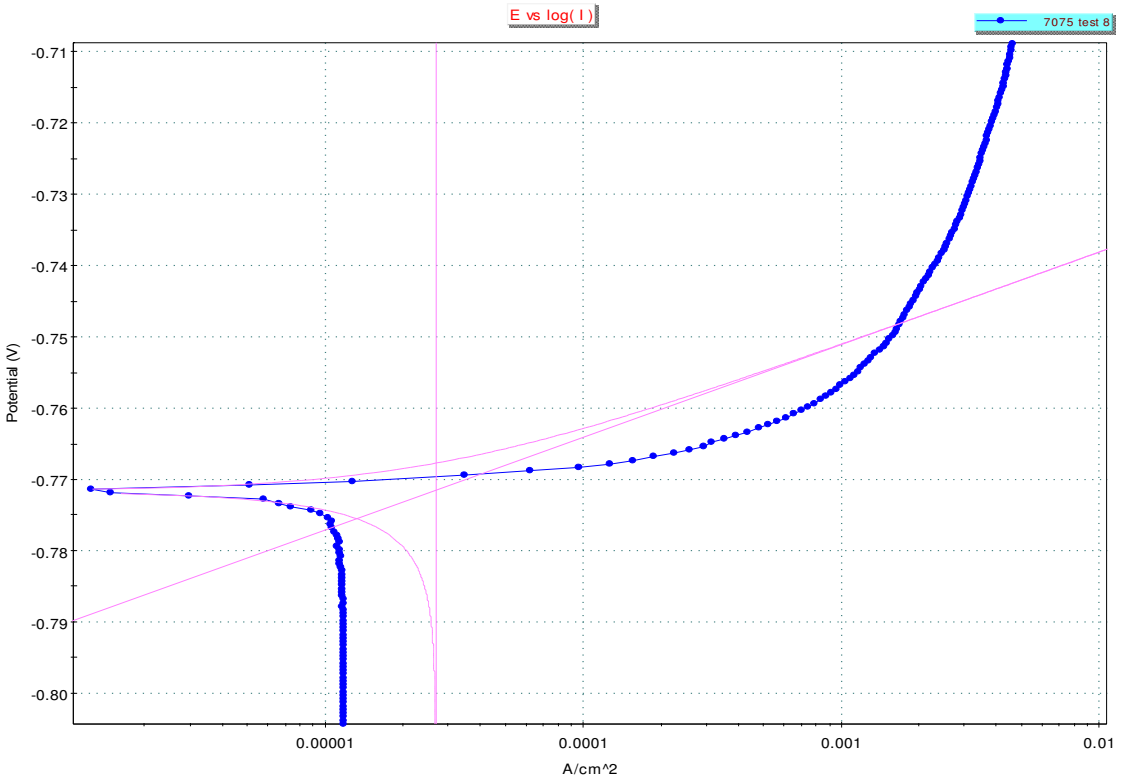
E vs log(I)
7075 test 8
-0.71
-0.72
-0.73
-0.74
-0.75
-0.76
-0.77
-0.78
-0.79
-0.80
Potential (V)
0.00001
0.0001
0.001
0.01
A/cm^2

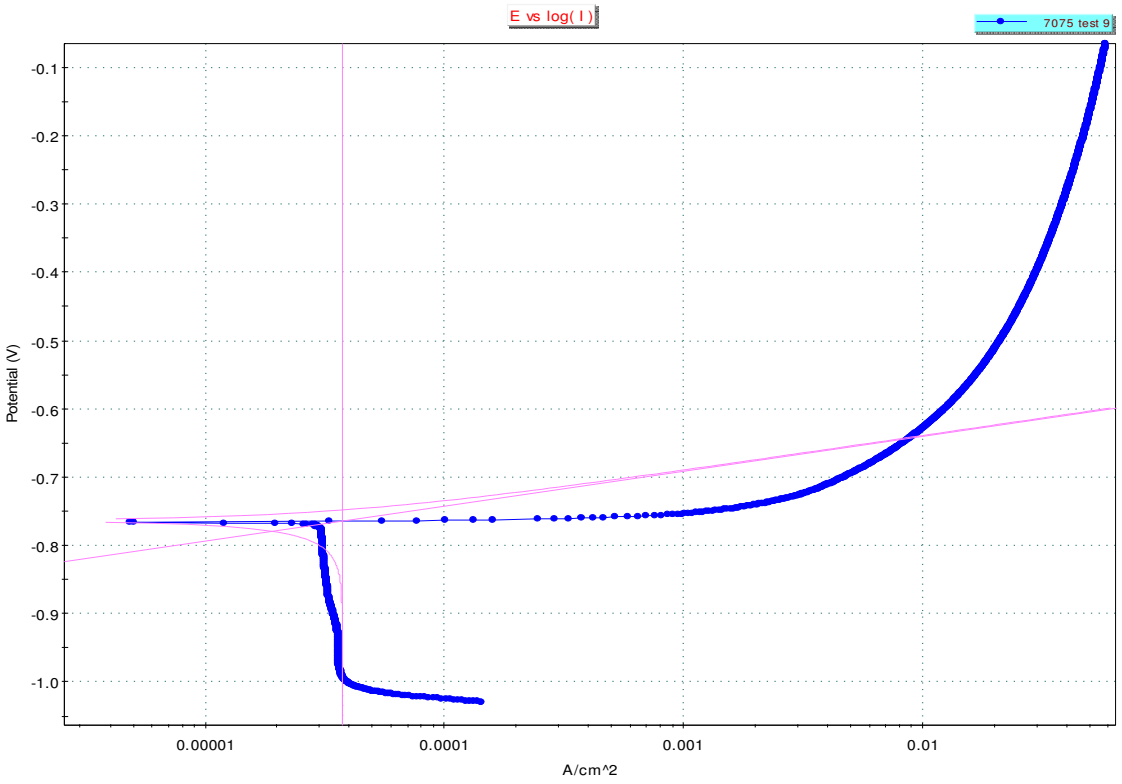

2195 Polarization Curves

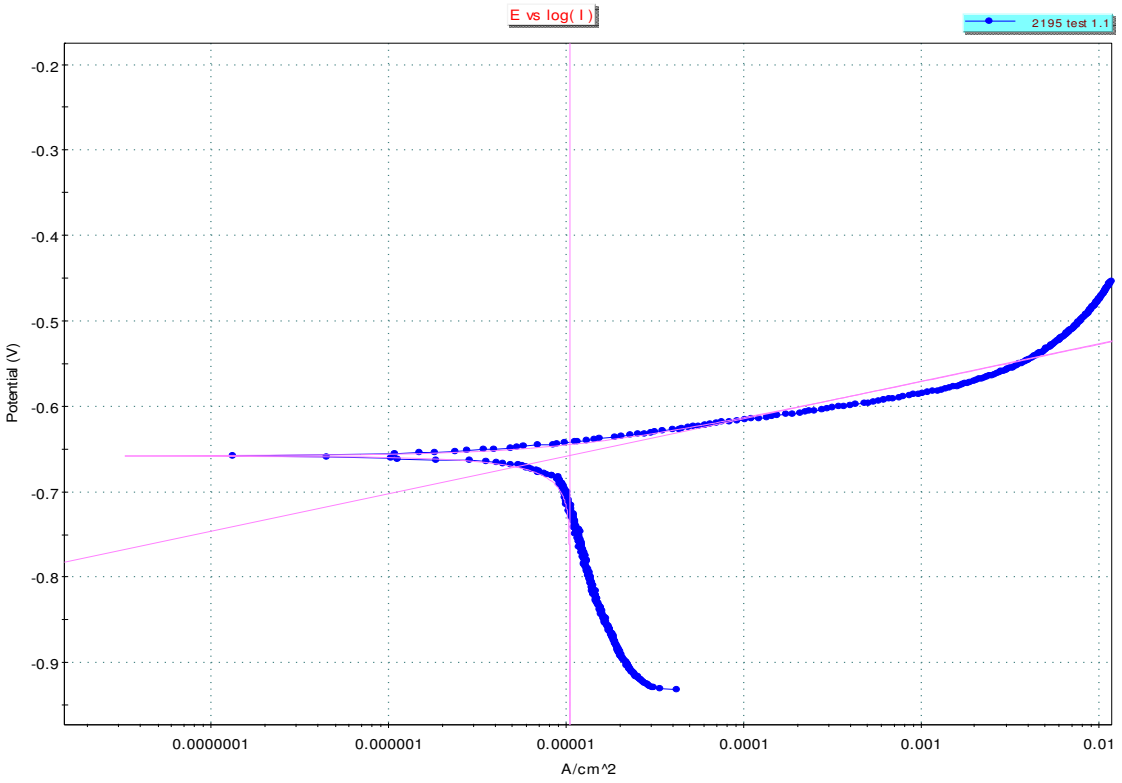

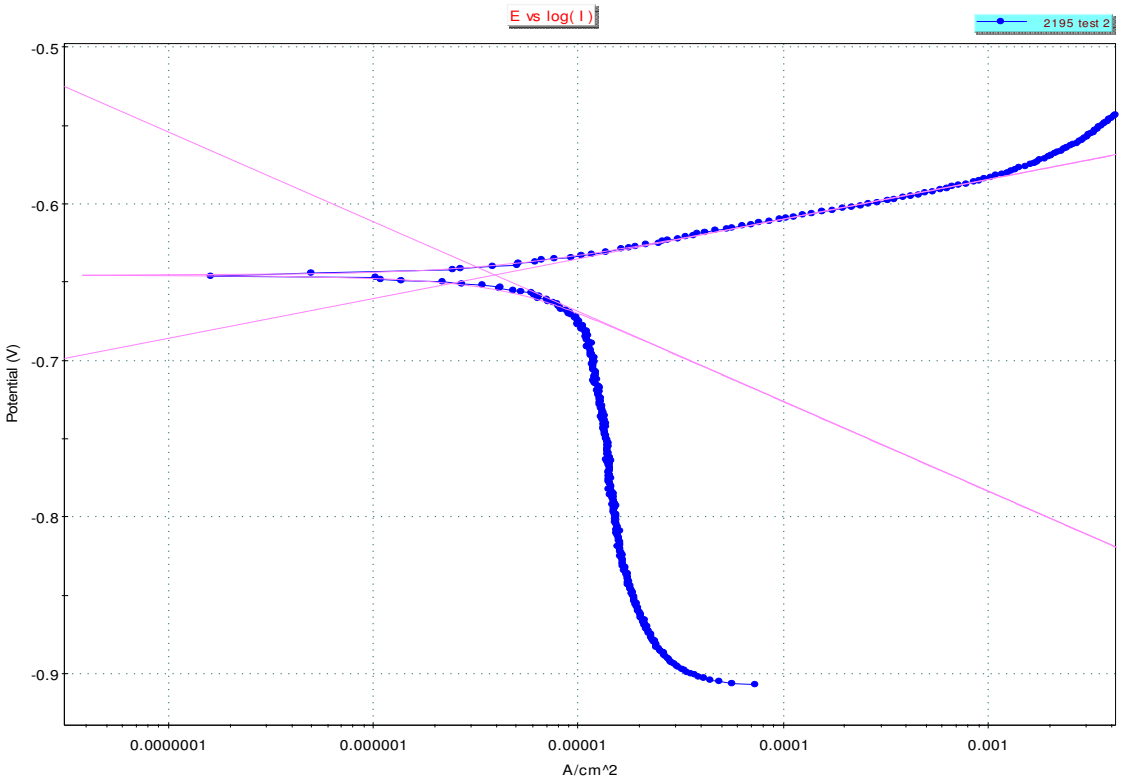
E vs log(I)
2195 test 2
-0.5
-0.6
-0.7
-0.8
-0.9
Potential (V)
0.0000001
0.000001
0.00001
0.0001
0.001
A/cm^2

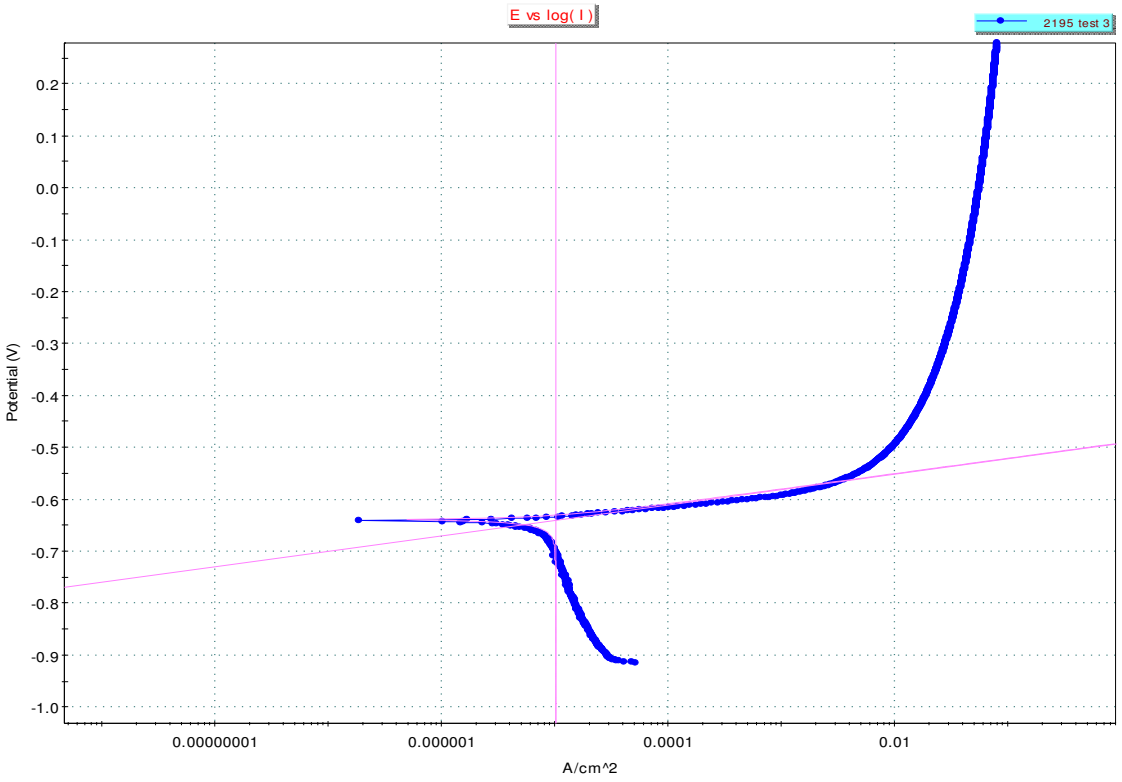
E vs log(I)
2195 test 3
0.2
0.1
0.0
-0.1
-0.2
-0.3
-0.4
-0.5
-0.6
-0.7
-0.8
-0.9
-1.0
Potential (V)
0.00000001
0.000001
0.0001
0.01
A/cm^2

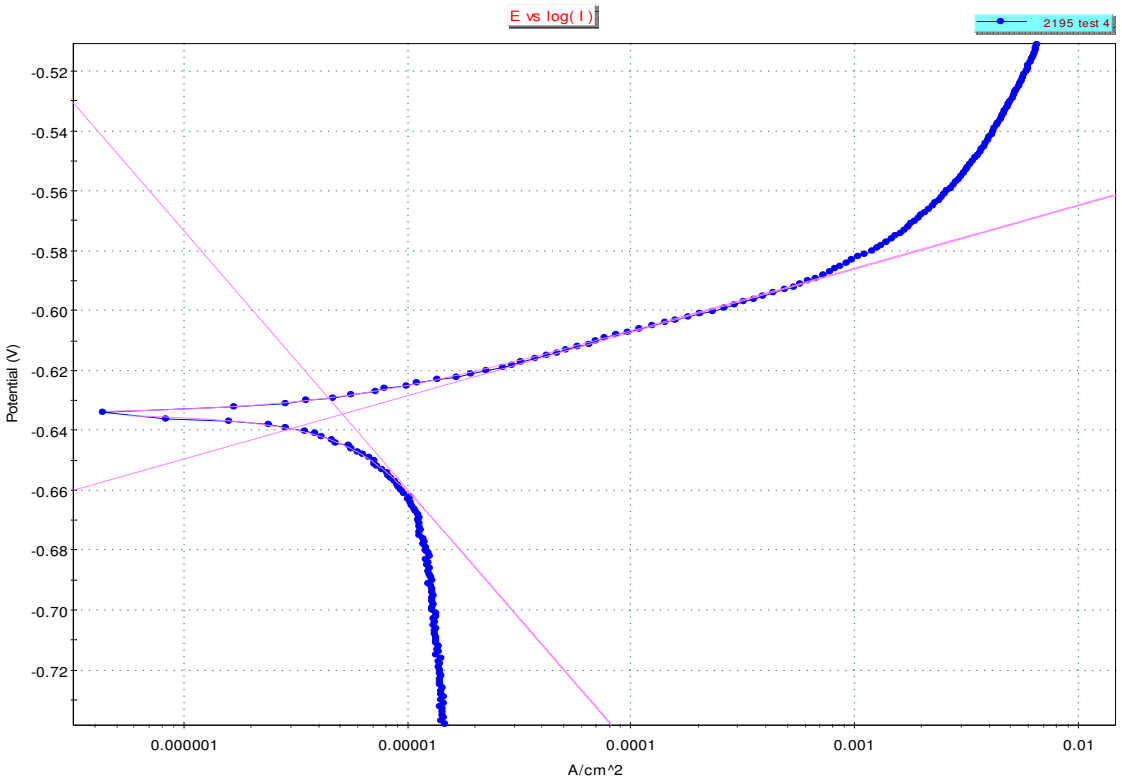
E vs log(I)
2195 test 4
-0.52
-0.54
-0.56
-0.58
-0.60
-0.62
-0.64
-0.66
-0.68
-0.70
-0.72
Potential (V)
0.000001
0.00001
0.0001
0.001
0.01
A/cm^2

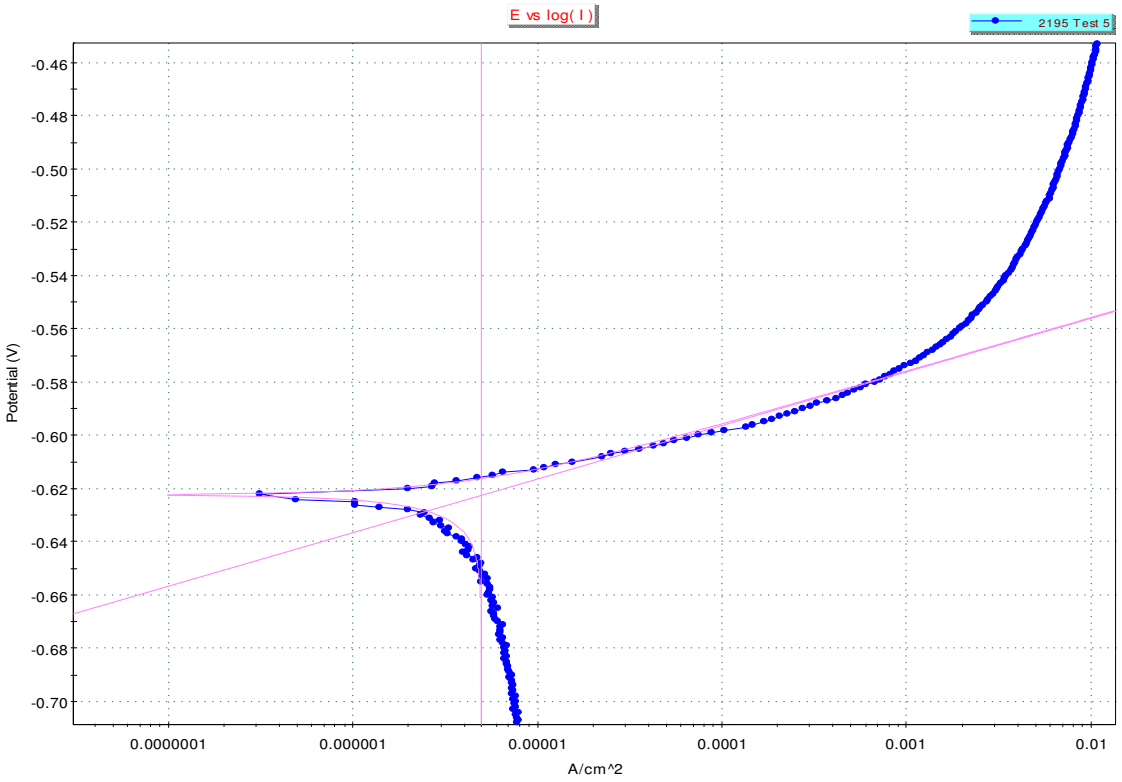
E vs log(I)
2195 Test 5
-0.46
-0.48
-0.50
-0.52
-0.54
-0.56
-0.58
-0.60
-0.62
-0.64
-0.66
-0.68
-0.70
Potential (V)
0.0000001
0.000001
0.00001
0.0001
0.001
0.01
A/cm^2

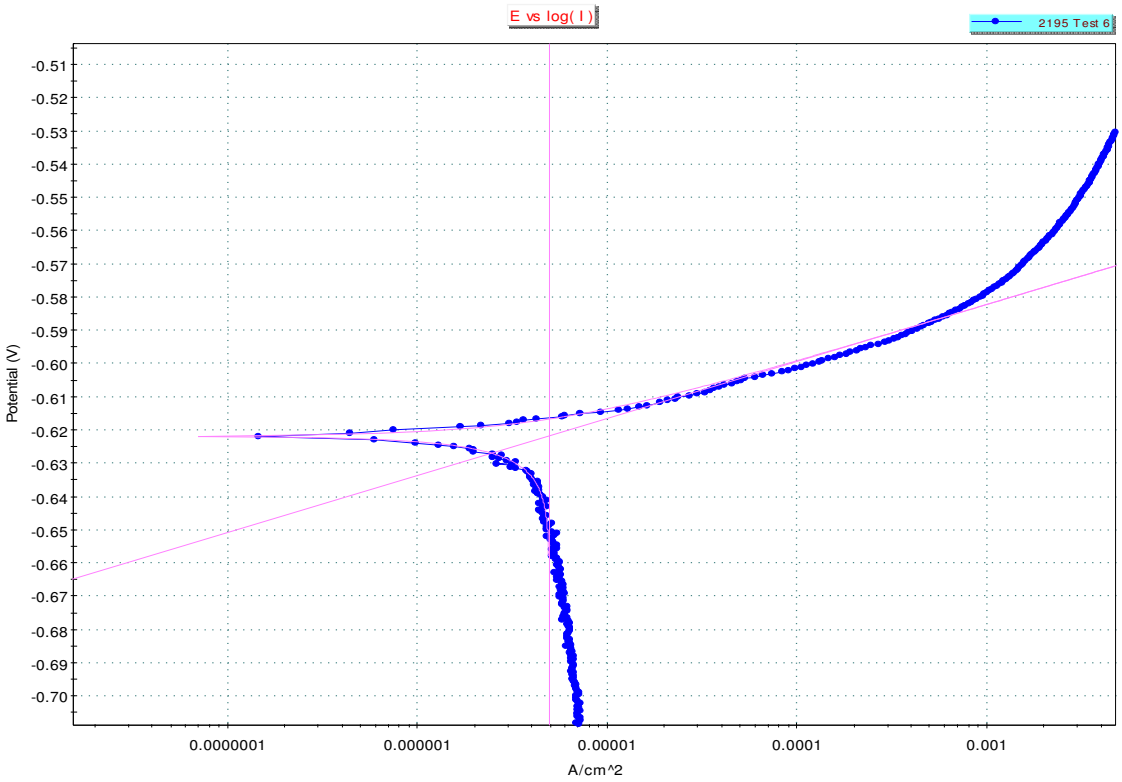
E vs log(I)
2195 Test 6
Potential (V)
-0.51
-0.52
-0.53
-0.54
-0.55
-0.56
-0.57
-0.58
-0.59
-0.60
-0.61
-0.62
-0.63
-0.64
-0.65
-0.66
-0.67
-0.68
-0.69
-0.70
0.0000001
0.000001
0.00001
0.0001
0.001
A/cm^2

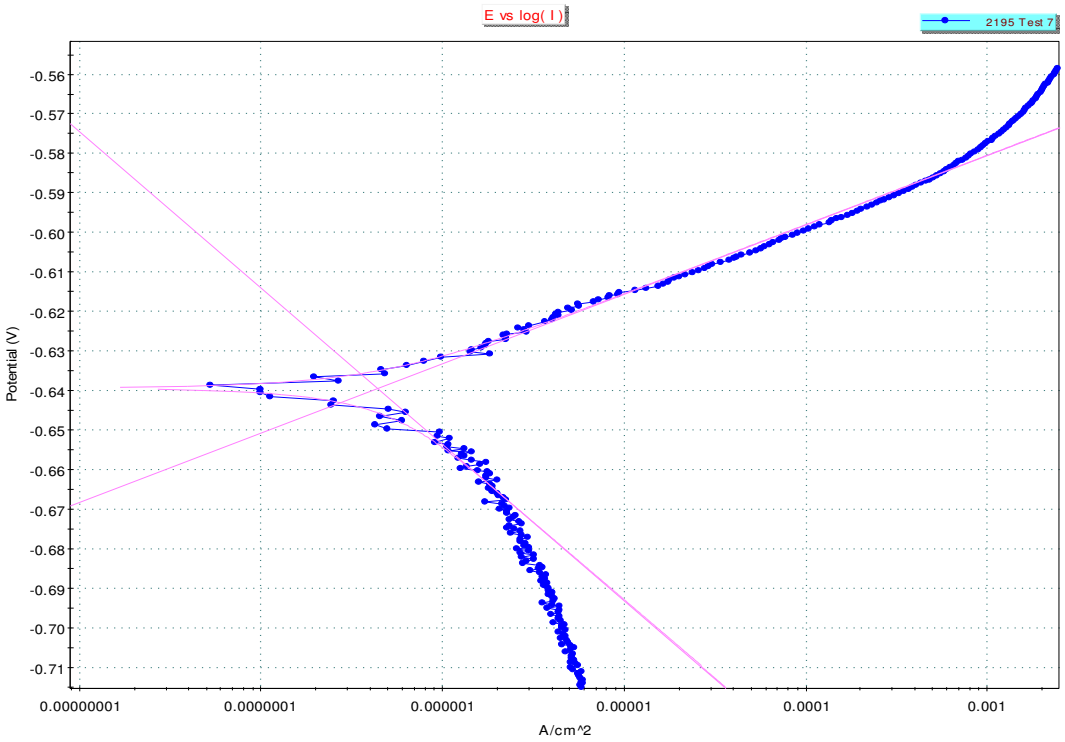
E vs log(I)
2195 Test 7
Potential (V)
-0.56
-0.57
-0.58
-0.59
-0.60
-0.61
-0.62
-0.63
-0.64
-0.65
-0.66
-0.67
-0.68
-0.69
-0.70
-0.71
0.00000001
0.0000001
0.000001
0.00001
0.0001
0.001
A/cm^2

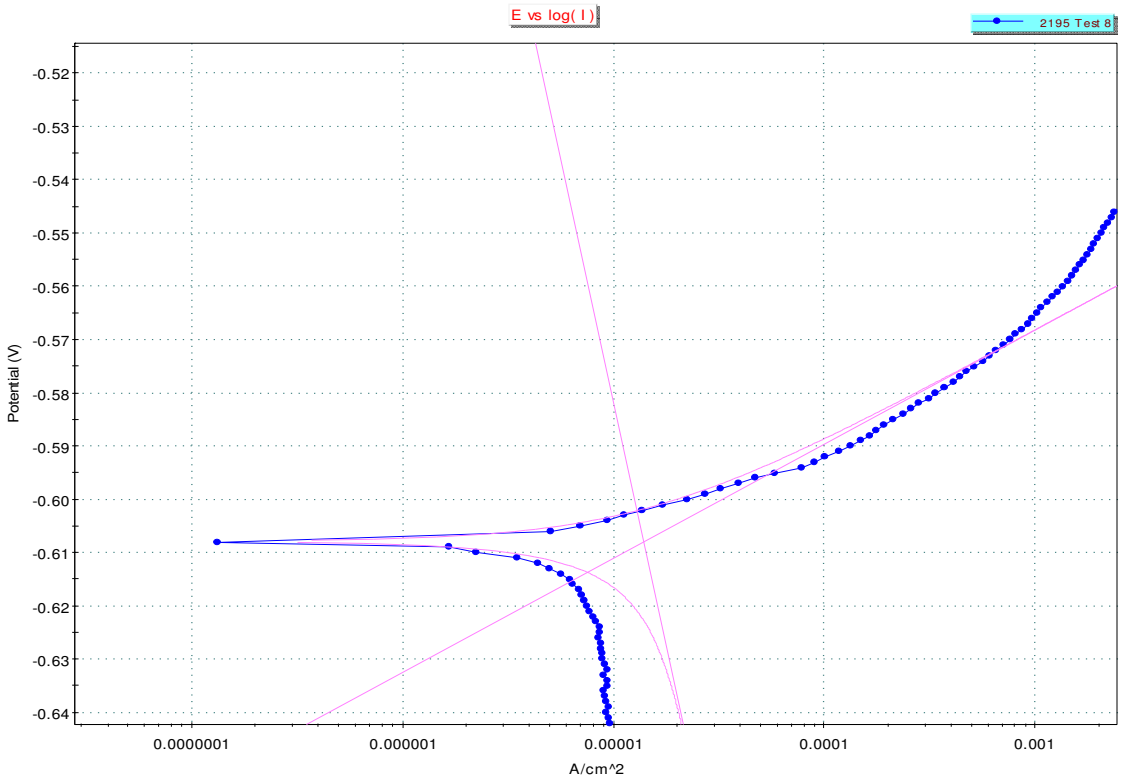
E vs log(I)
2195 Test 8
-0.52
-0.53
-0.54
-0.55
-0.56
-0.57
-0.58
-0.59
-0.60
-0.61
-0.62
-0.63
-0.64
Potential (V)
0.0000001
0.000001
0.00001
0.0001
0.001
A/cm^2

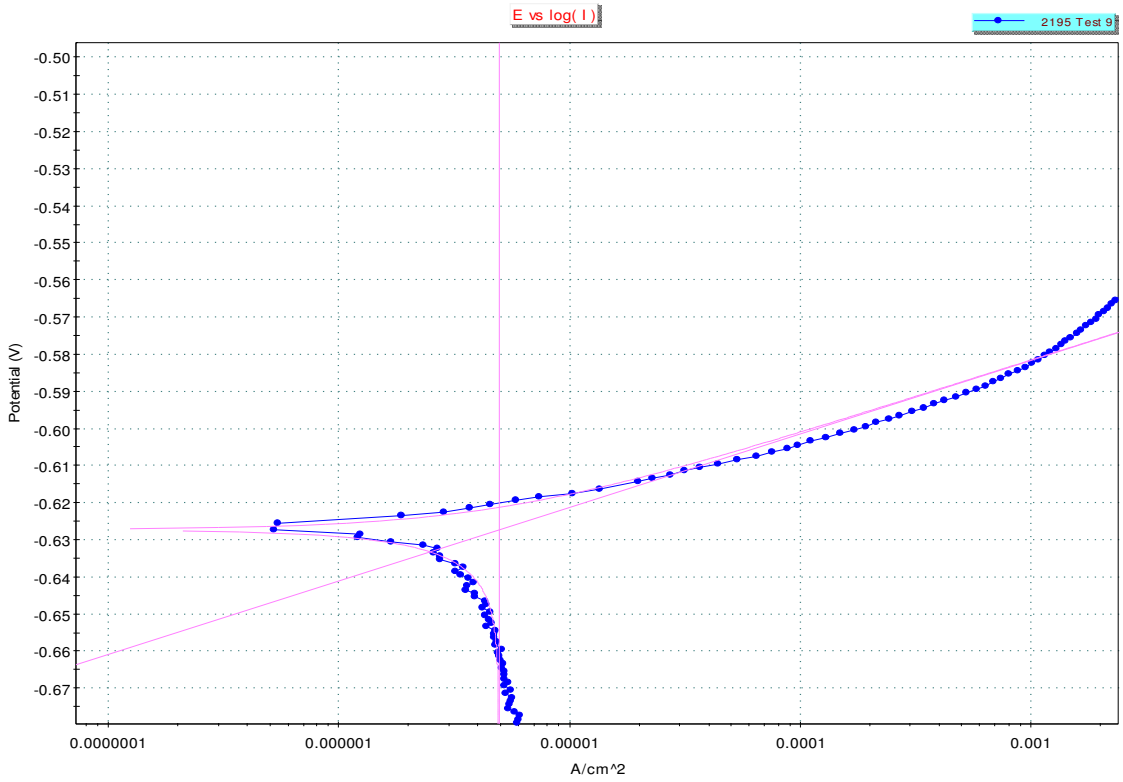
E vs log(I)
2195 Test 9
-0.50
-0.51
-0.52
-0.53
-0.54
-0.55
-0.56
-0.57
-0.58
-0.59
-0.60
-0.61
-0.62
-0.63
-0.64
-0.65
-0.66
-0.67
Potential (V)
0.0000001
0.000001
0.00001
0.0001
0.001
A/cm^2

2050 T3 Polarization Curves

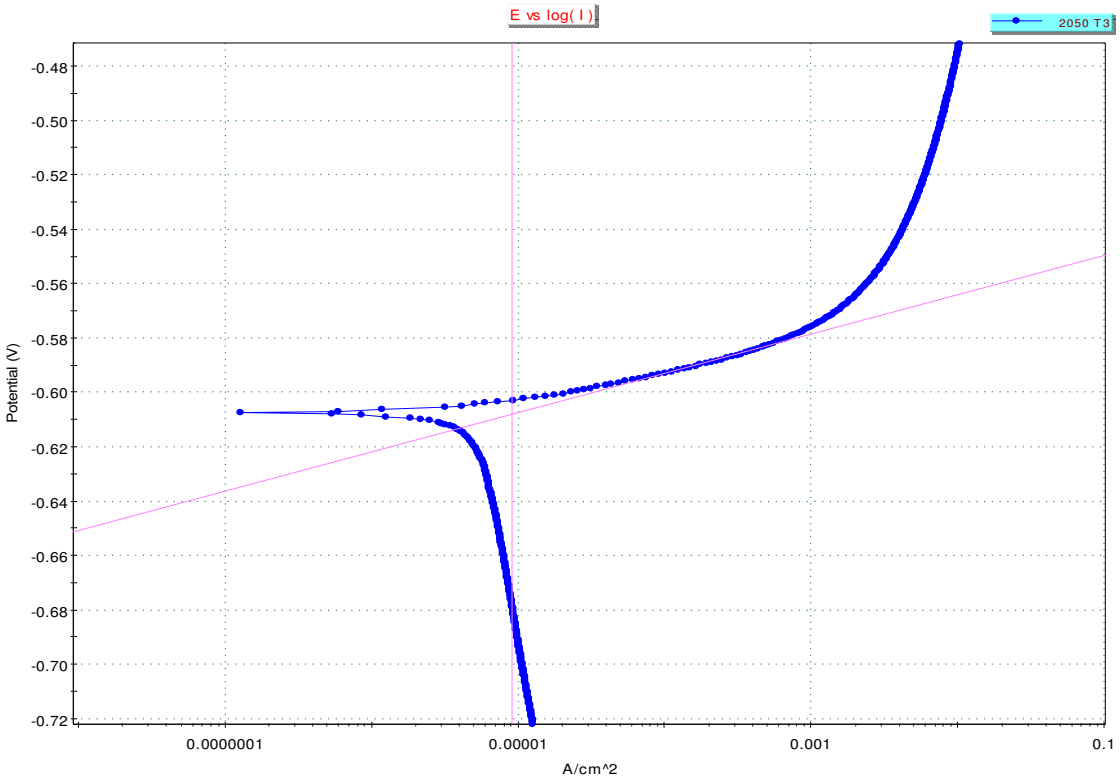

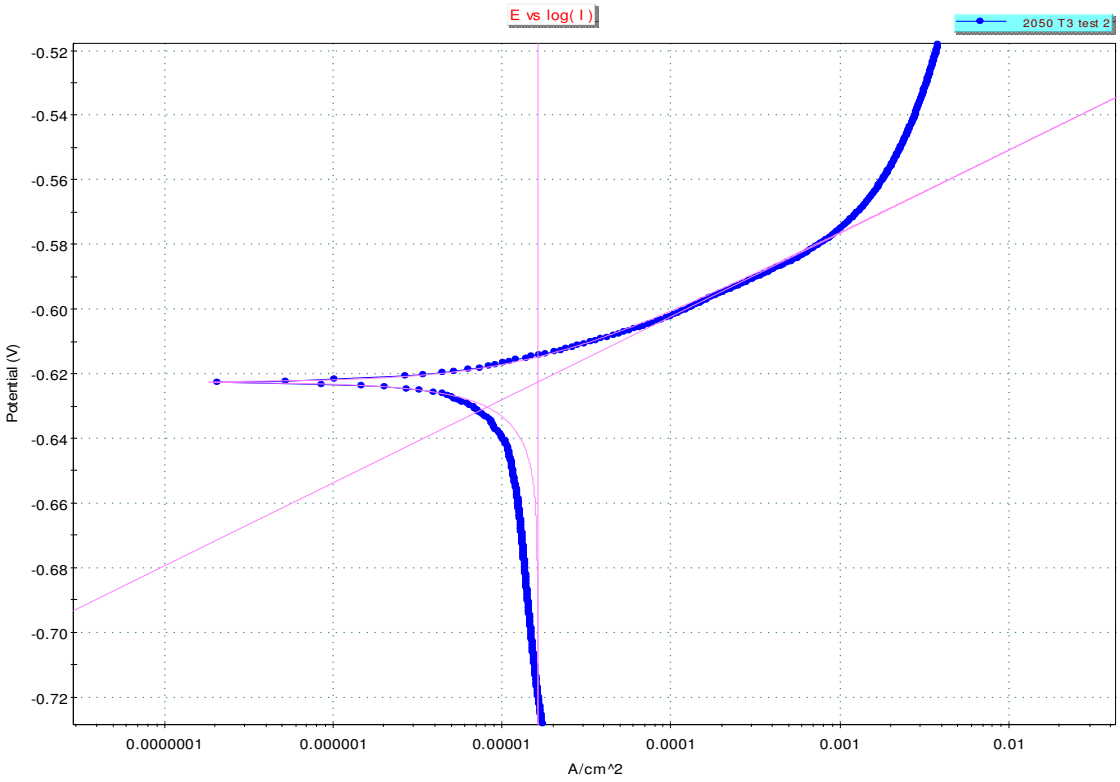

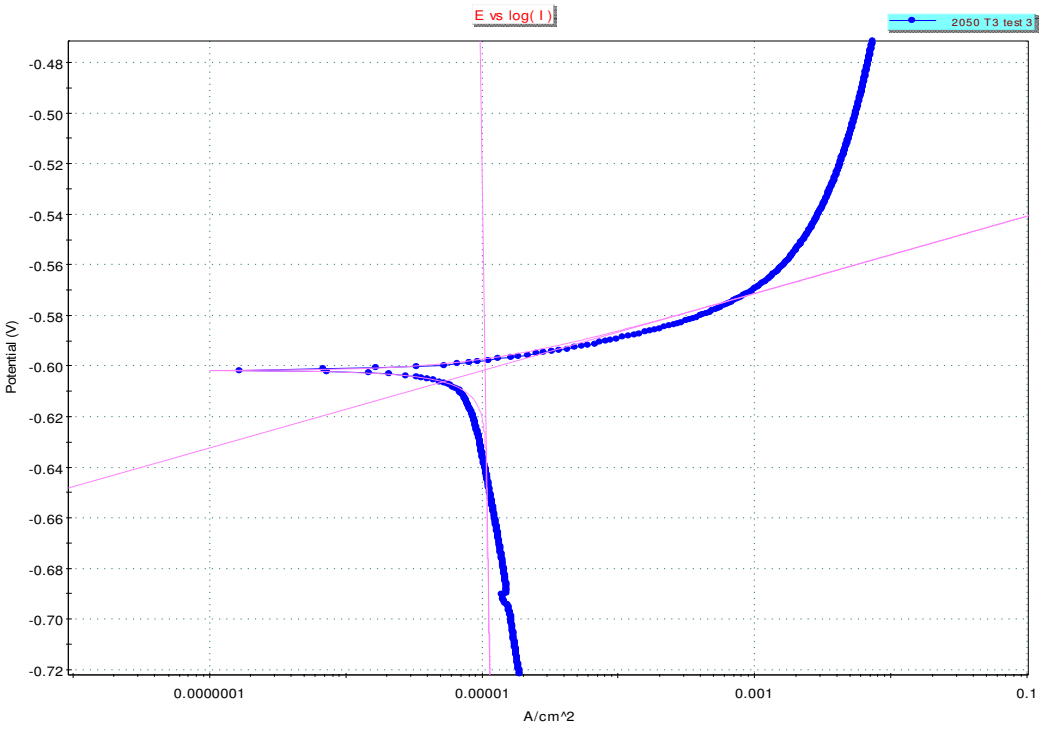
E vs log(I)
2050 T3 test 3
-0.48
-0.50
-0.52
-0.54
-0.56
-0.58
-0.60
-0.62
-0.64
-0.66
-0.68
-0.70
-0.72
Potential (V)
0.0000001
0.00001
0.001
0.1
A/cm^2

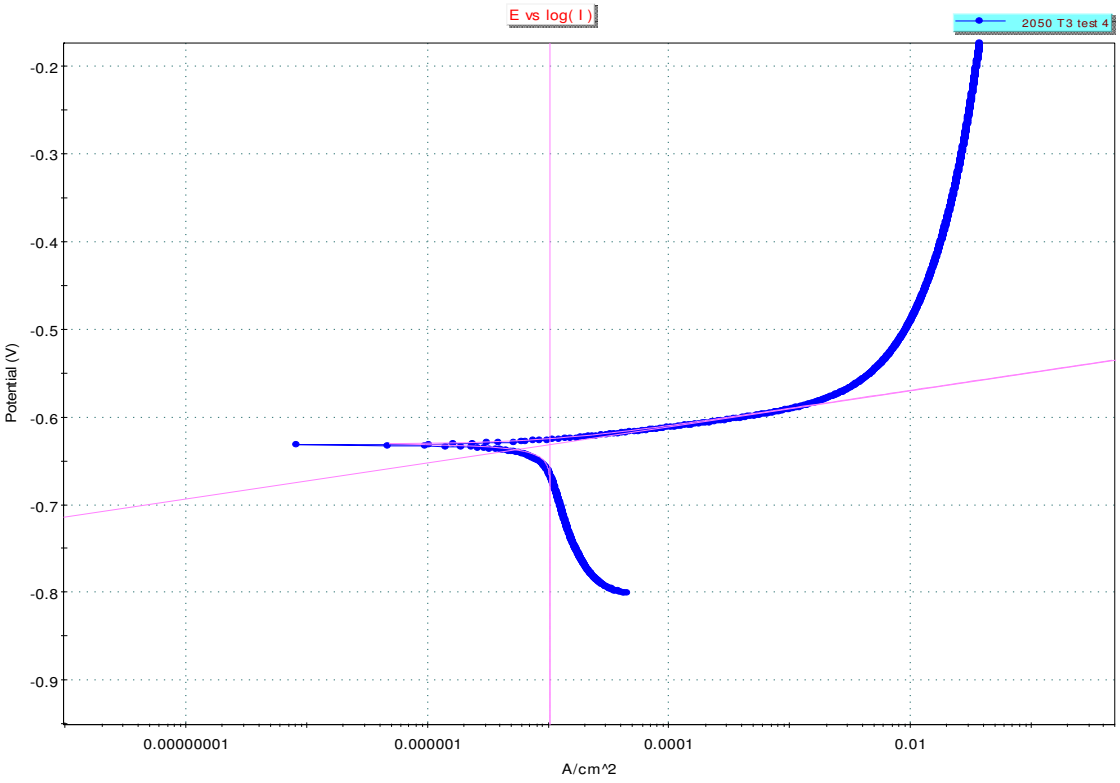
E vs log(I)
2050 T3 test 4
-0.2
-0.3
-0.4
-0.5
-0.6
-0.7
-0.8
-0.9
Potential (V)
0.00000001
0.000001
0.0001
0.01
A/cm^2

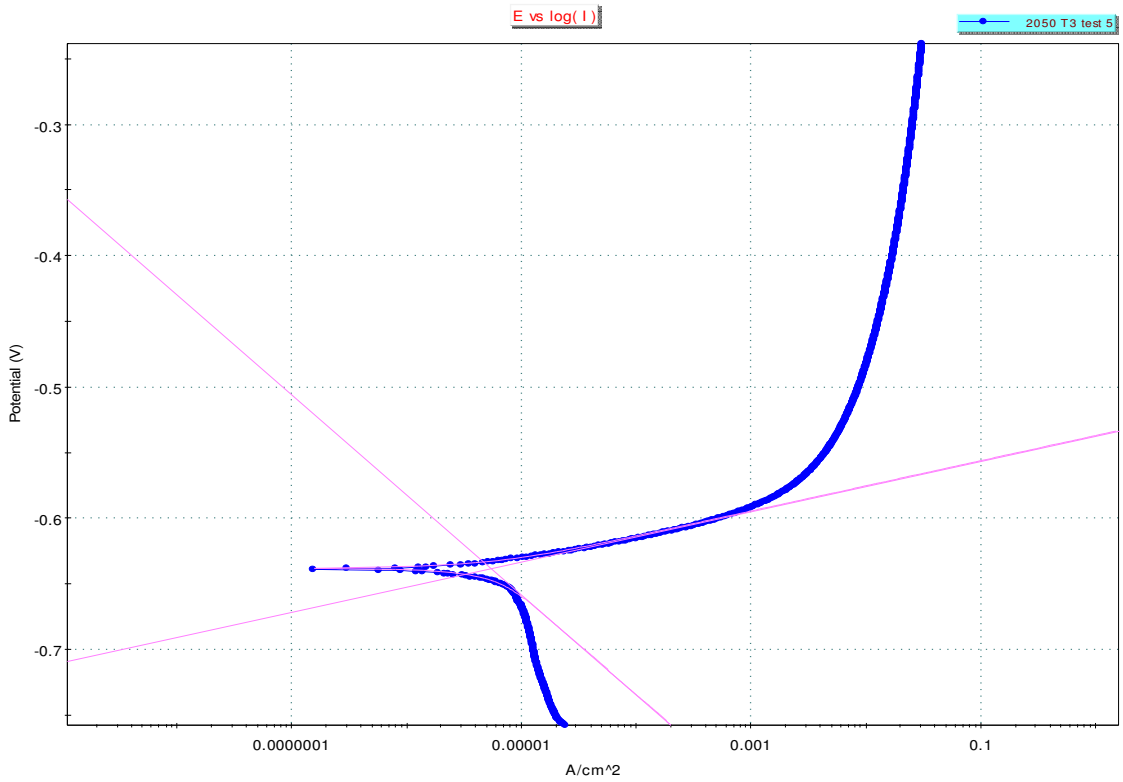
E vs log(I)
2050 T3 test 5
-0.3
-0.4
-0.5
-0.6
-0.7
Potential (V)
0.0000001
0.00001
0.001
0.1
A/cm^2

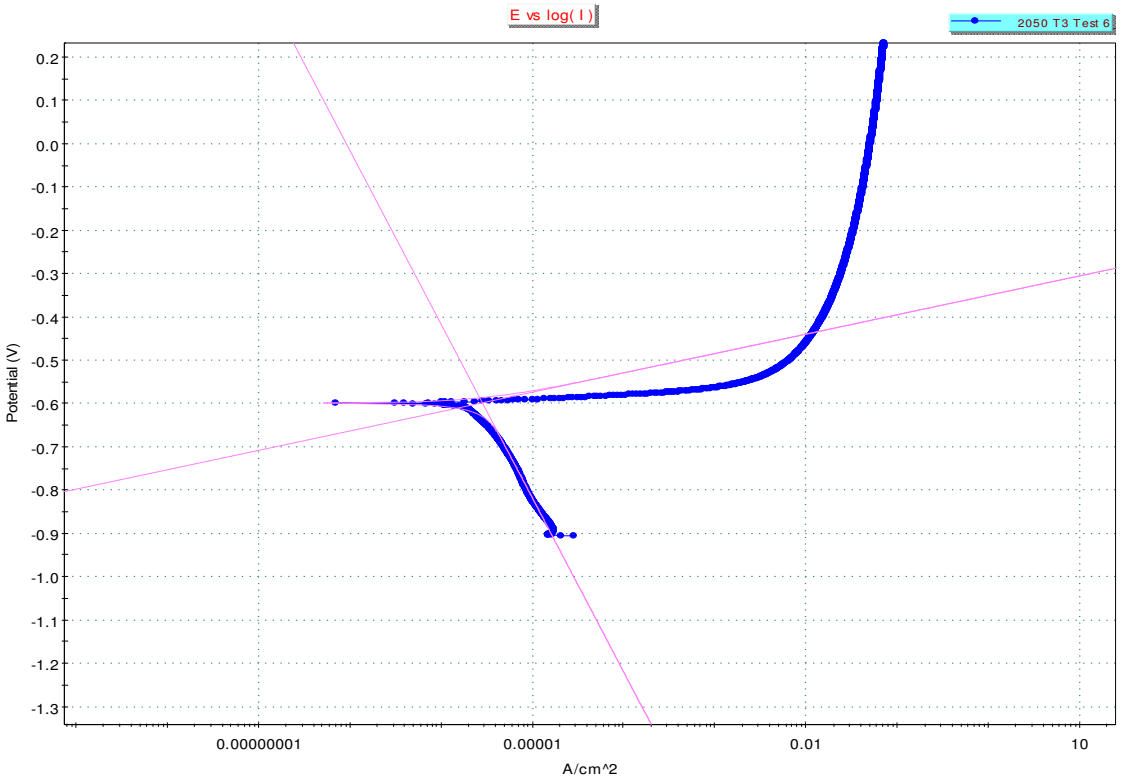
E vs log(I)
2050 T3 Test 6
0.2
0.1
0.0
-0.1
-0.2
-0.3
-0.4
-0.5
-0.6
-0.7
-0.8
-0.9
-1.0
-1.1
-1.2
-1.3
Potential (V)
0.00000001
0.00001
0.01
10
A/cm^2

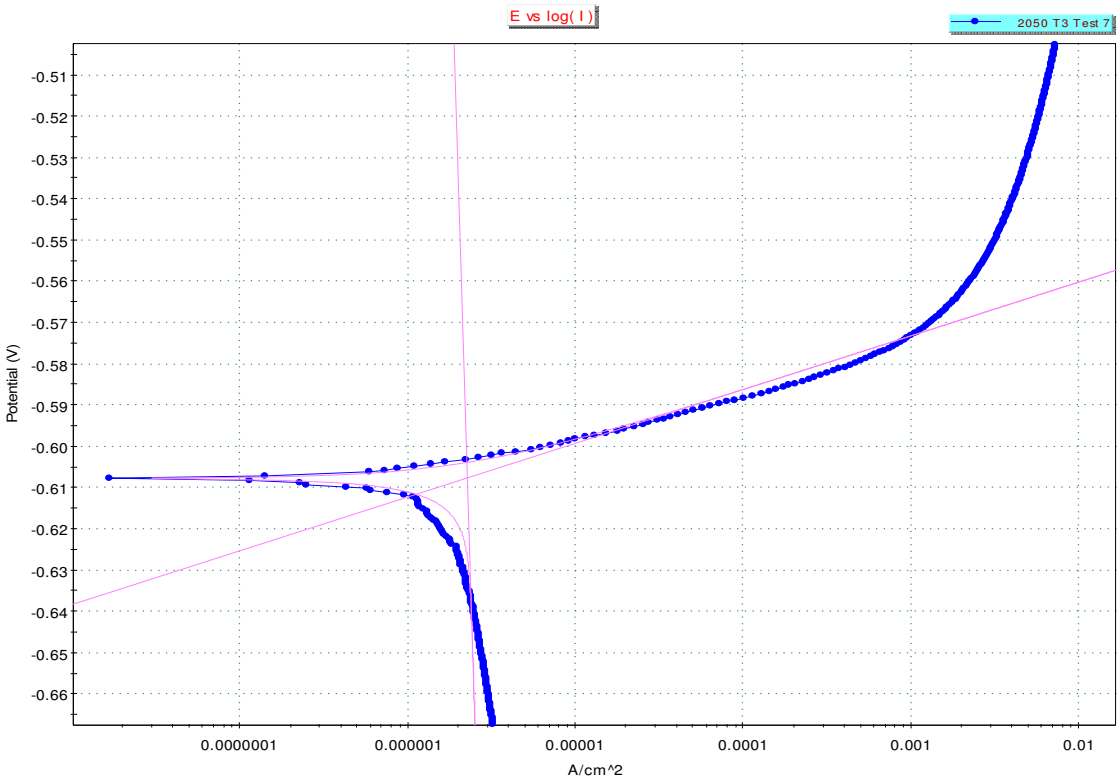
E vs log(I)
2050 T3 Test 7
Potential (V)
-0.51
-0.52
-0.53
-0.54
-0.55
-0.56
-0.57
-0.58
-0.59
-0.60
-0.61
-0.62
-0.63
-0.64
-0.65
-0.66
0.0000001
0.000001
0.00001
0.0001
0.001
0.01
A/cm^2

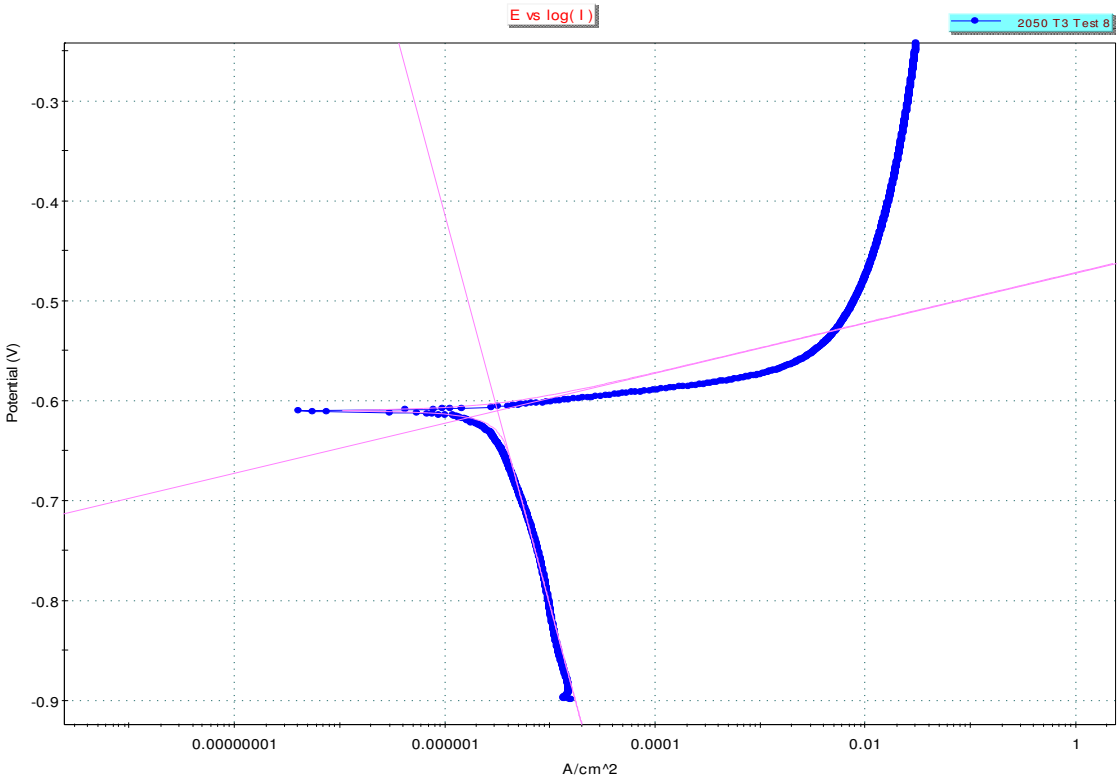
E vs log(I)
2050 T3 Test 8
Potential (V)
-0.3
-0.4
-0.5
-0.6
-0.7
-0.8
-0.9
0.00000001
0.000001
0.0001
0.01
1
A/cm^2

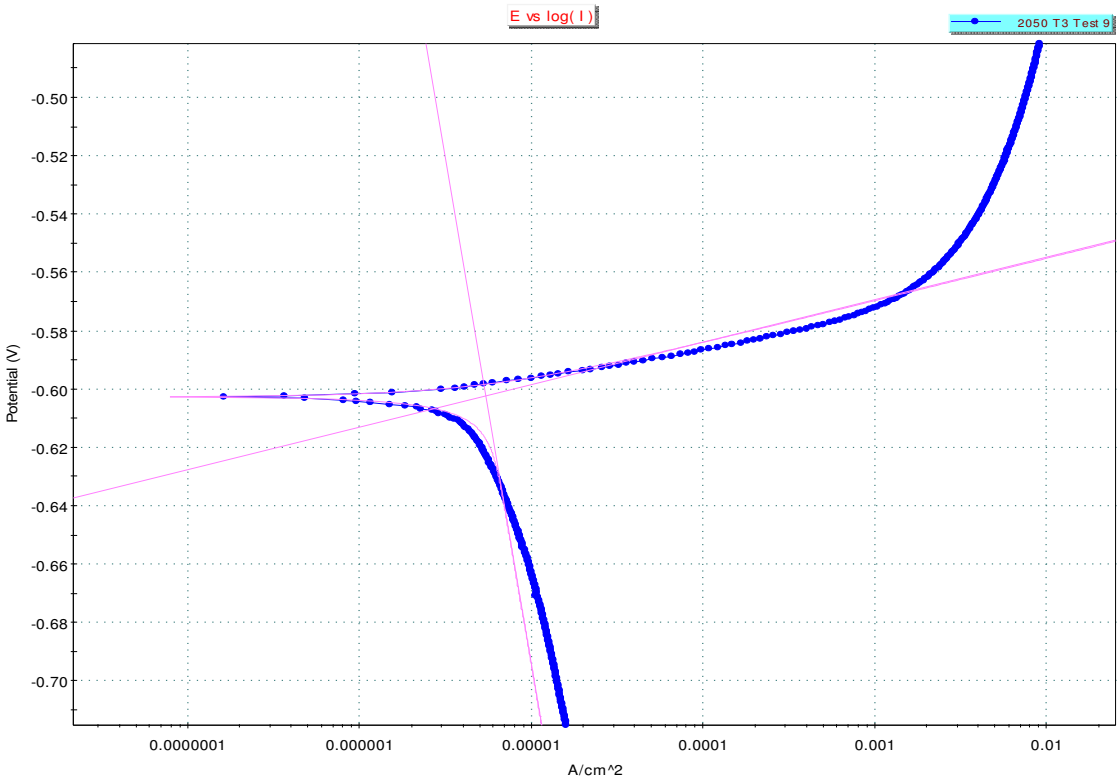

2050 T852 Polarization Curves

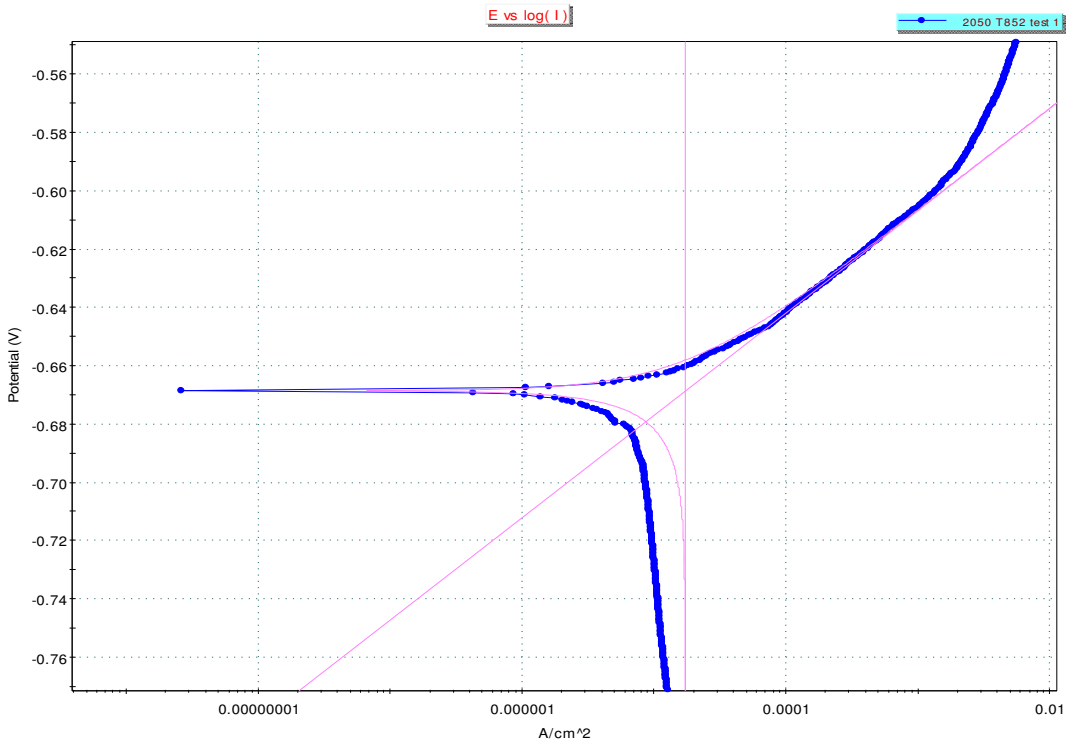

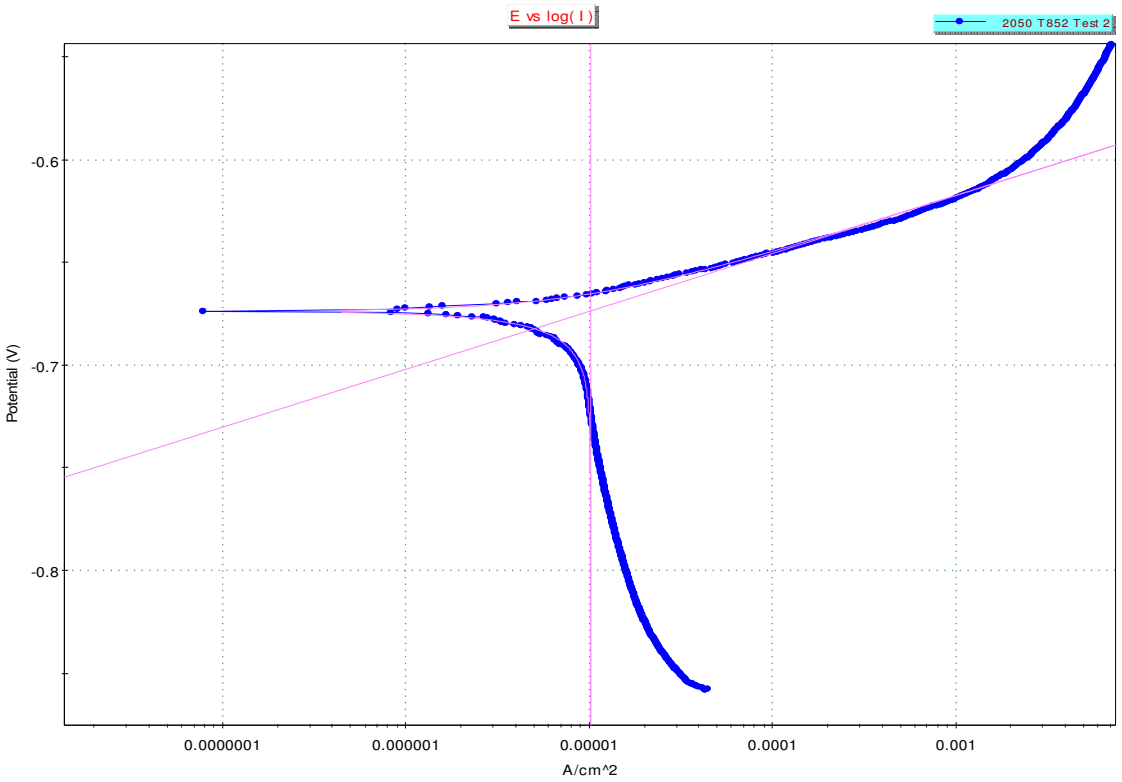
E vs log(I)
2050 T852 Test 2
-0.6
-0.7
-0.8
Potential (V)
0.0000001
0.000001
0.00001
0.0001
0.001
A/cm^2

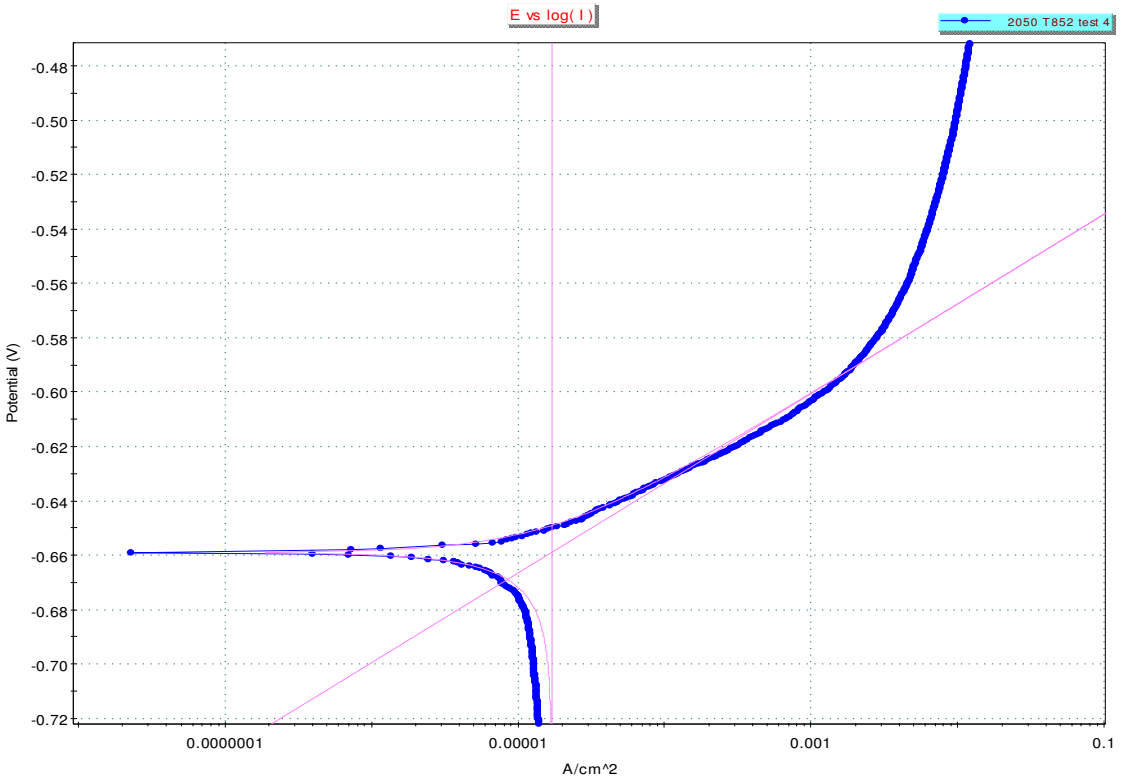
E vs log(I)
2050 T852 test 4
-0.48
-0.50
-0.52
-0.54
-0.56
-0.58
-0.60
-0.62
-0.64
-0.66
-0.68
-0.70
-0.72
Potential (V)
0.0000001
0.00001
0.001
0.1
A/cm^2

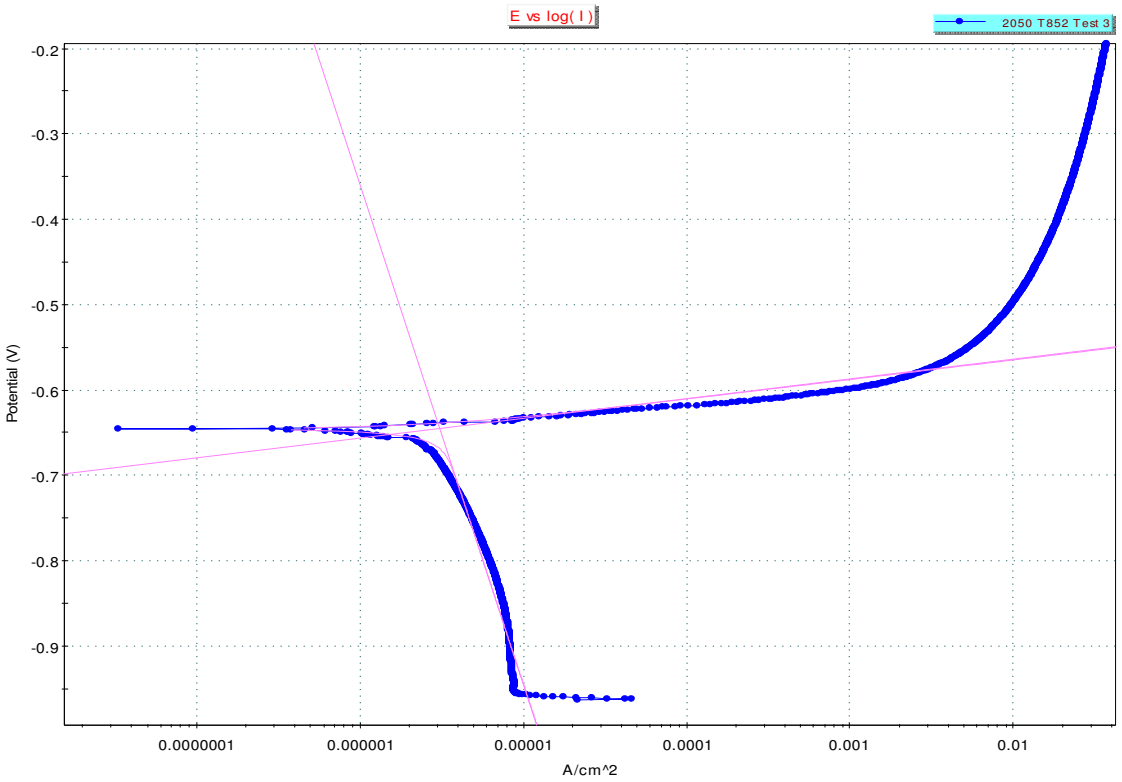
E vs log(I)
2050 T852 Test 3
-0.2
-0.3
-0.4
-0.5
-0.6
-0.7
-0.8
-0.9
Potential (V)
0.0000001
0.000001
0.00001
0.0001
0.001
0.01
A/cm^2

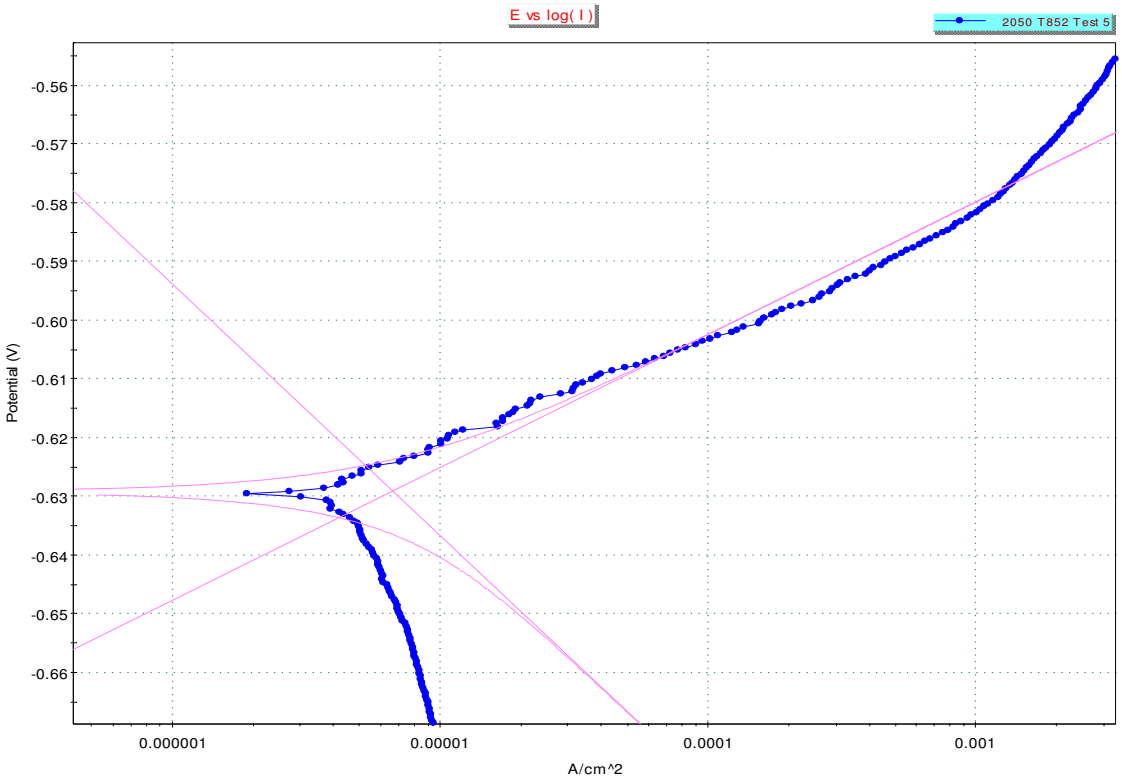
E vs log(I)
2050 T852 Test 5
-0.56
-0.57
-0.58
-0.59
-0.60
-0.61
-0.62
-0.63
-0.64
-0.65
-0.66
Potential (V)
0.000001
0.00001
0.0001
0.001
A/cm^2

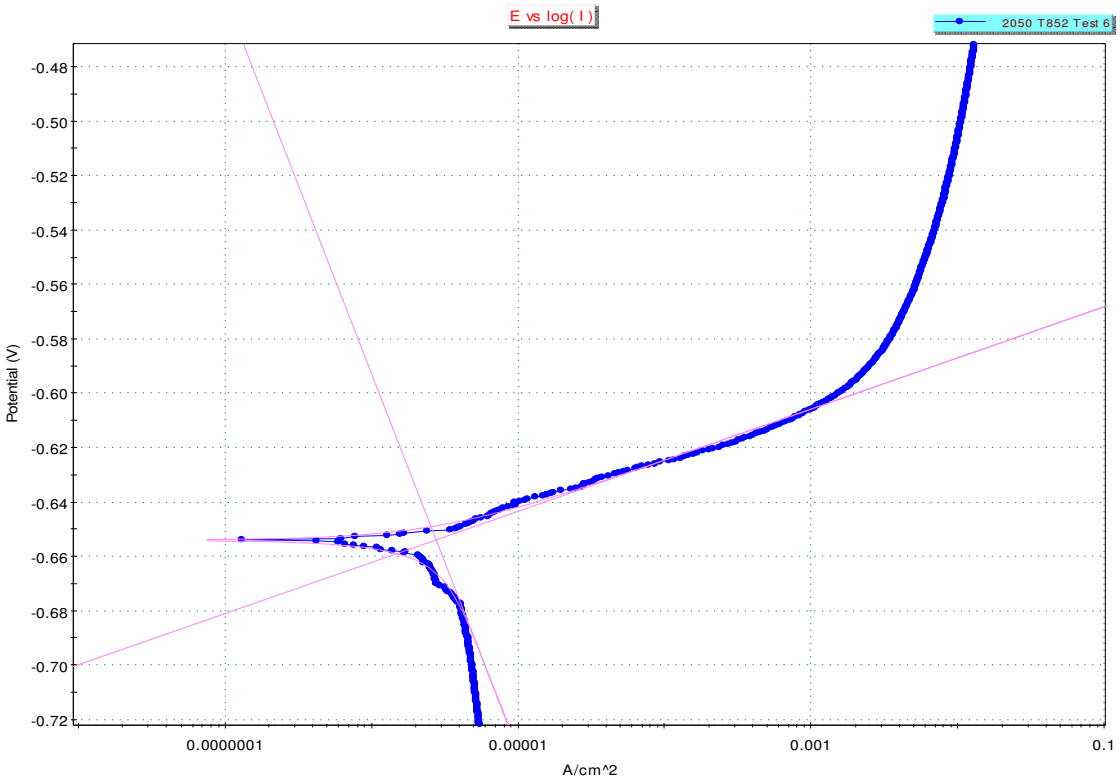
E vs log(I)
2050 T852 Test 6
-0.48
-0.50
-0.52
-0.54
-0.56
-0.58
-0.60
-0.62
-0.64
-0.66
-0.68
-0.70
-0.72
Potential (V)
0.0000001
0.00001
0.001
0.1
A/cm^2

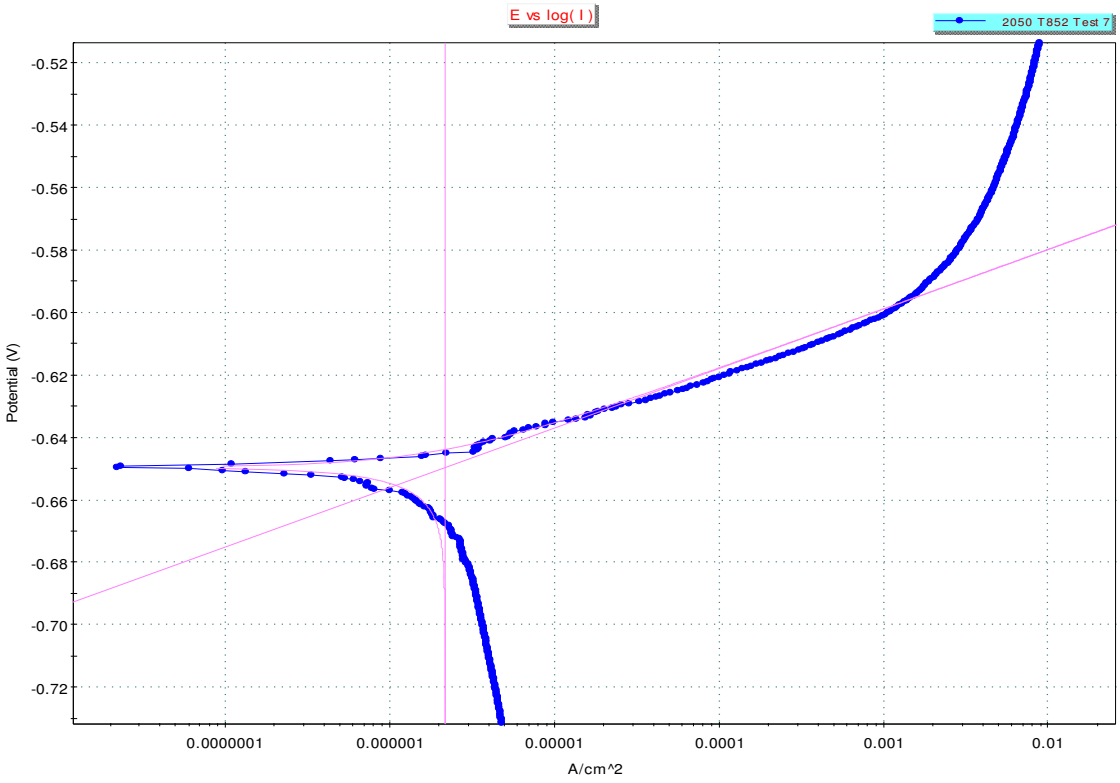
E vs log(I)
2050 T852 Test 7
-0.52
-0.54
-0.56
-0.58
-0.60
-0.62
-0.64
-0.66
-0.68
-0.70
-0.72
Potential (V)
0.0000001
0.000001
0.00001
0.0001
0.001
0.01
A/cm^2

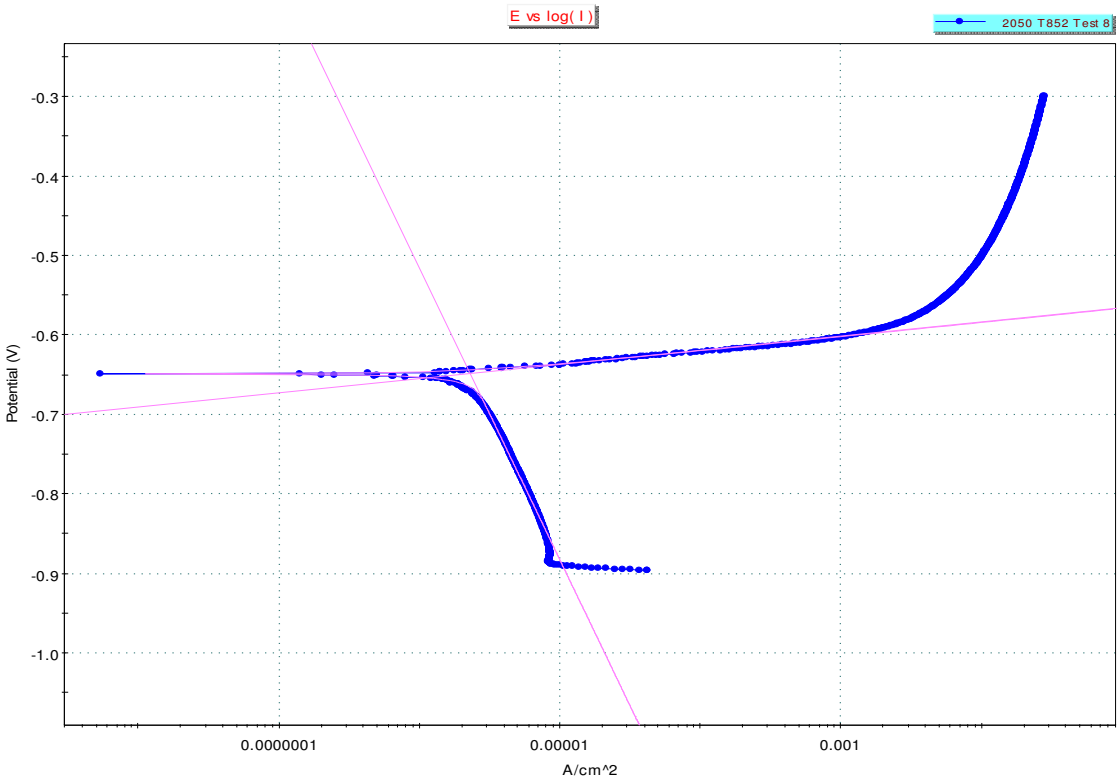
E vs log(I)
2050 T852 Test 8
-0.3
-0.4
-0.5
-0.6
-0.7
-0.8
-0.9
-1.0
Potential (V)
0.0000001
0.00001
0.001
A/cm^2

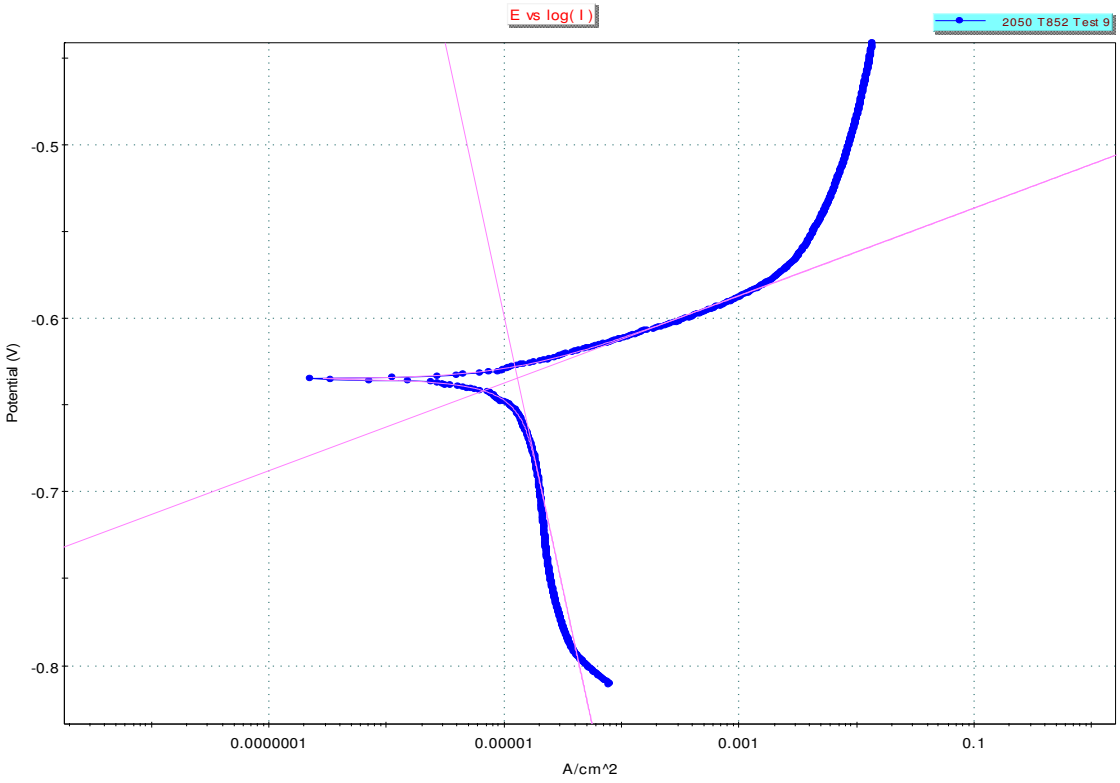
E vs log(I)
2050 T852 Test 9
-0.5
-0.6
-0.7
-0.8
Potential (V)
0.0000001
0.00001
0.001
0.1
A/cm^2

Ti-6Al-4V Polarization Curves

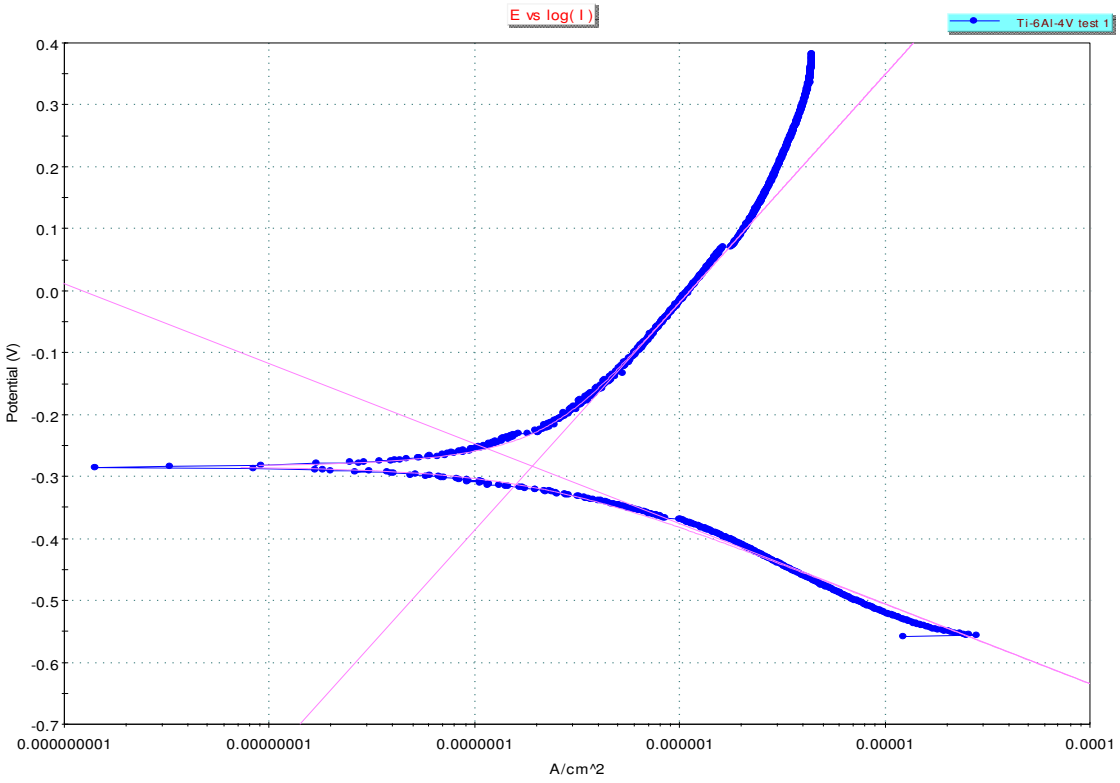

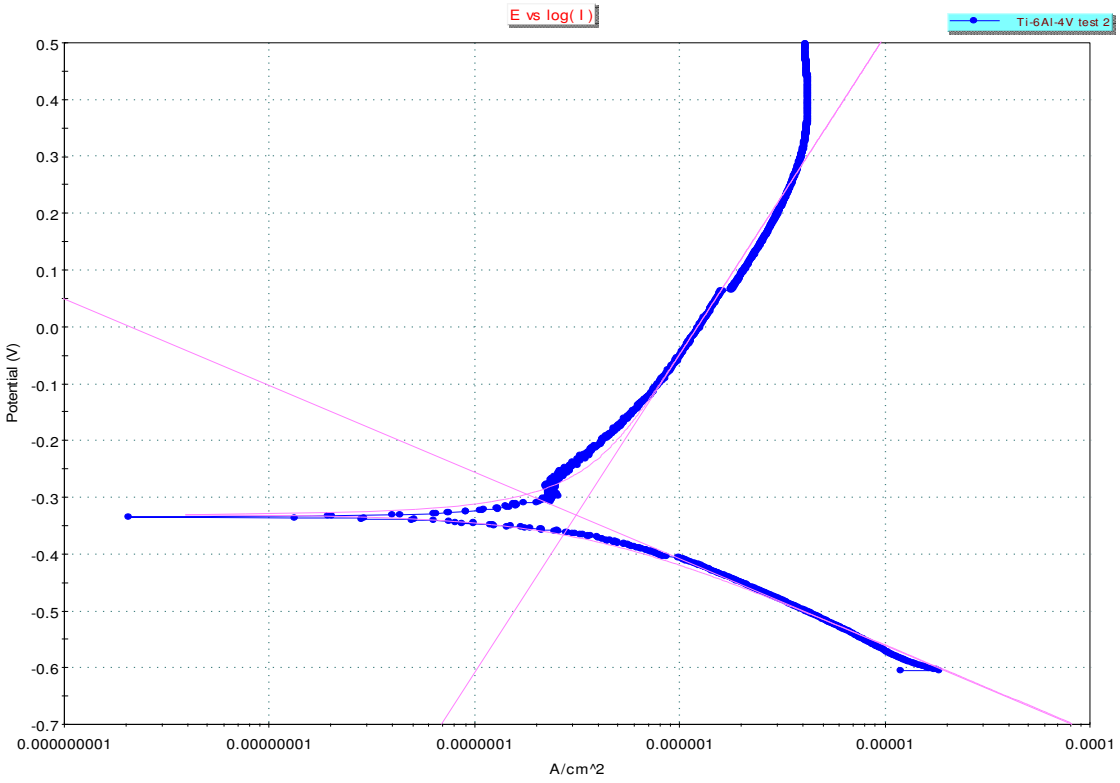

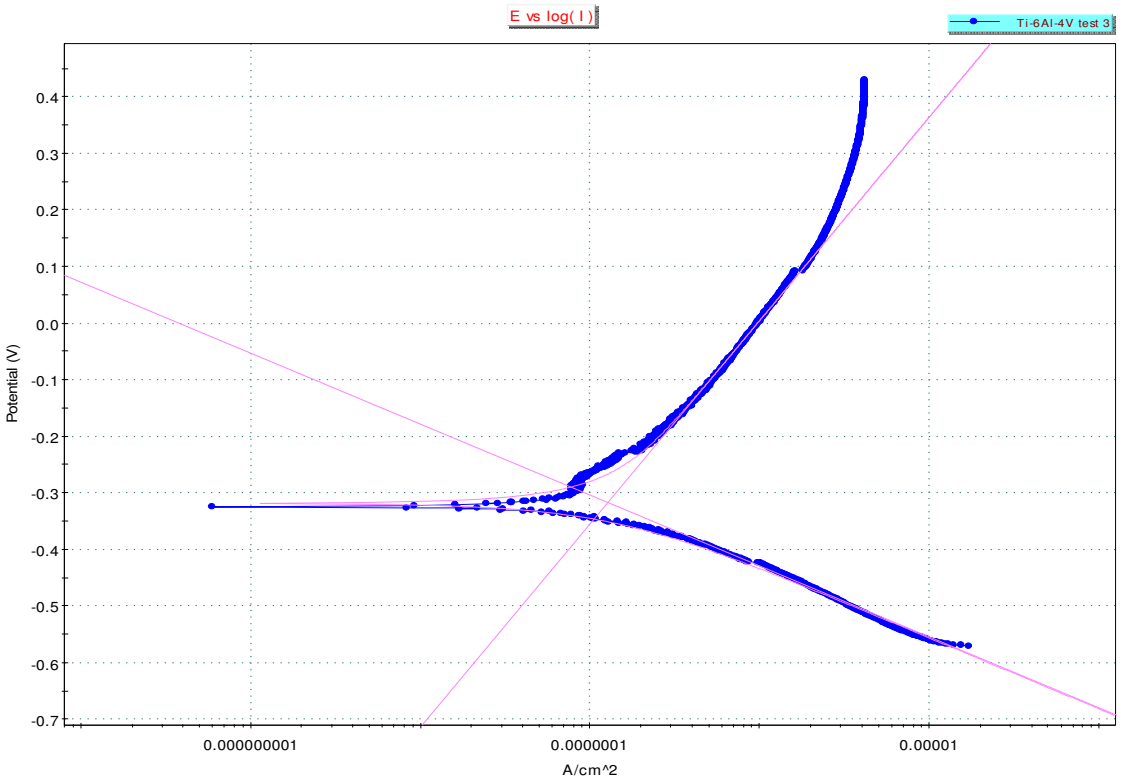
E vs log(I)
Ti-6Al-4V test 3
0.4
0.3
0.2
0.1
0.0
-0.1
-0.2
-0.3
-0.4
-0.5
-0.6
-0.7
Potential (V)
0.000000001
0.0000001
0.00001
A/cm^2

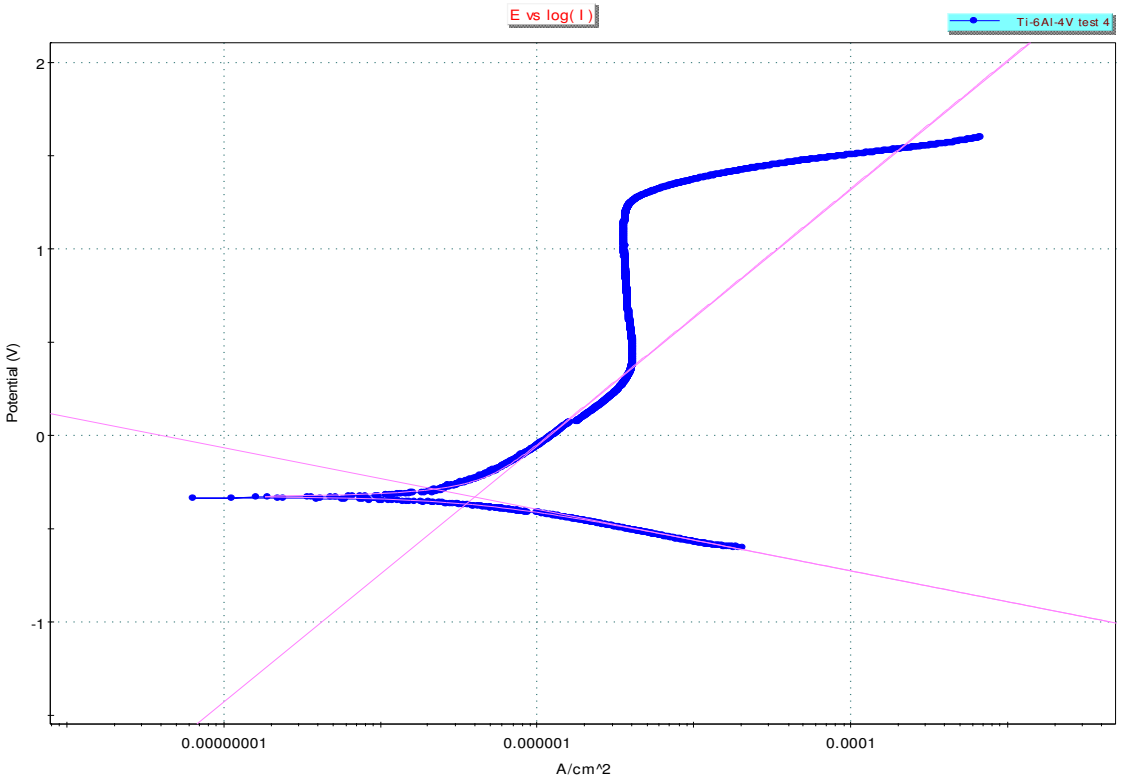
E vs log(I)
Ti-6Al-4V test 4
2
1
0
-1
Potential (V)
0.00000001
0.000001
0.0001
A/cm^2

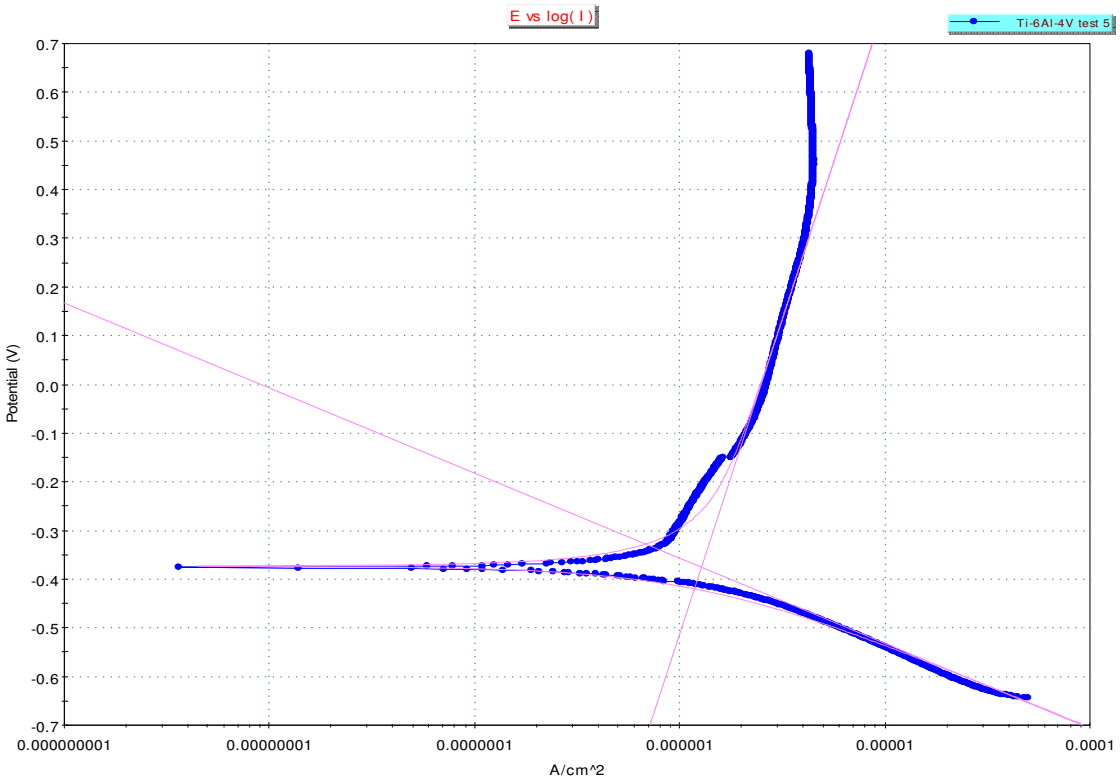
E vs log(I)
Ti-6Al-4V test 5
Potential (V)
0.7
0.6
0.5
0.4
0.3
0.2
0.1
0.0
-0.1
-0.2
-0.3
-0.4
-0.5
-0.6
-0.7
0.000000001
0.00000001
0.0000001
0.000001
0.00001
0.0001
A/cm^2

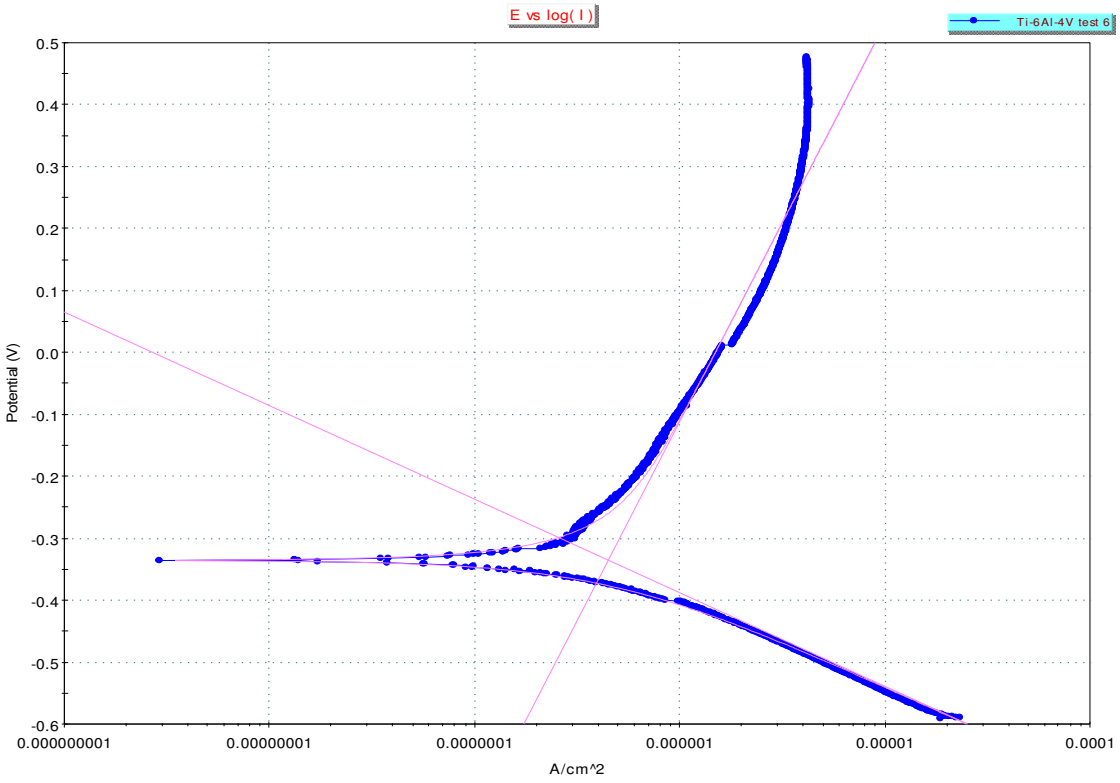
E vs log(I)
Ti-6Al-4V test 6
Potential (V)
0.5
0.4
0.3
0.2
0.1
0.0
-0.1
-0.2
-0.3
-0.4
-0.5
-0.6
0.000000001
0.00000001
0.0000001
0.000001
0.00001
0.0001
A/cm^2

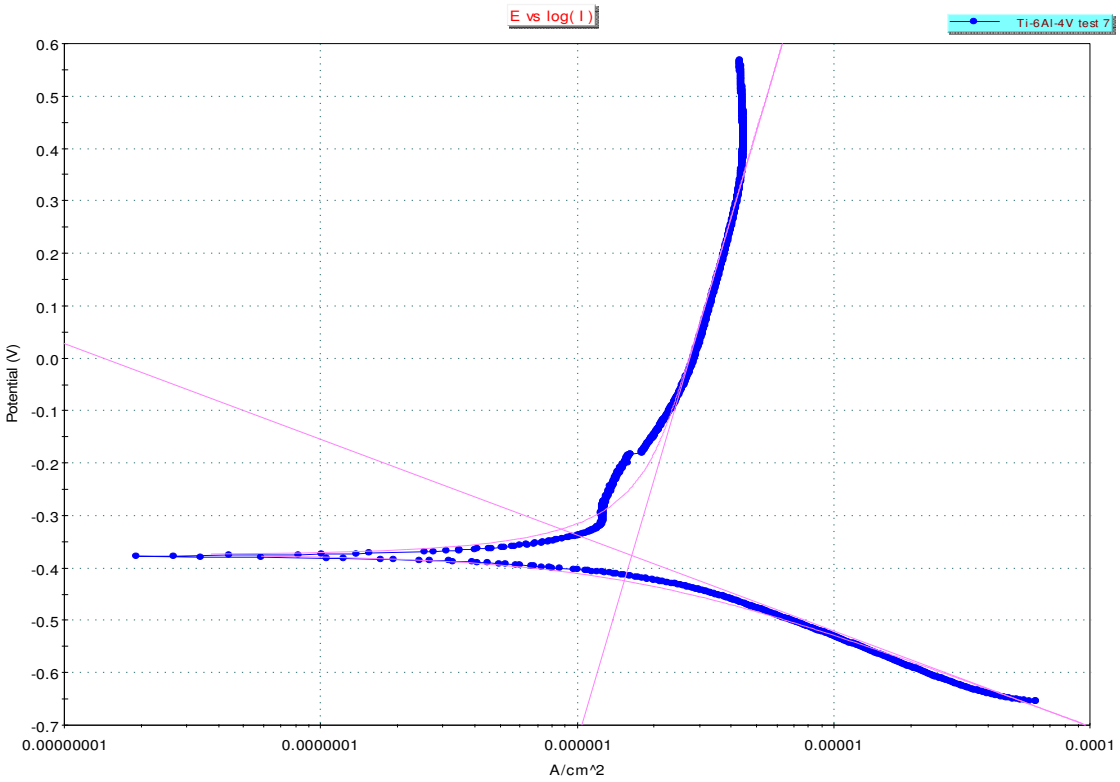
E vs log(I)
Ti-6Al-4V test 7
Potential (V)
0.6
0.5
0.4
0.3
0.2
0.1
0.0
-0.1
-0.2
-0.3
-0.4
-0.5
-0.6
-0.7
0.00000001
0.0000001
0.000001
0.00001
0.0001
A/cm^2

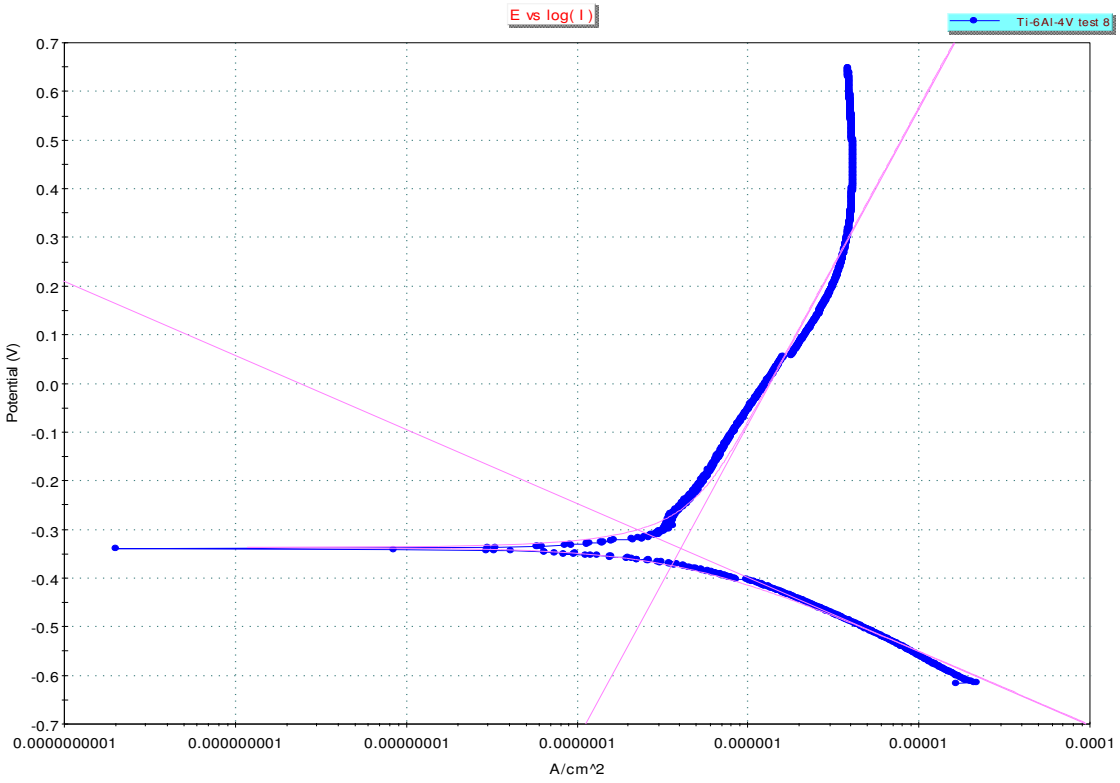
E vs log(I)
Ti-6Al-4V test 8
Potential (V)
0.7
0.6
0.5
0.4
0.3
0.2
0.1
0.0
-0.1
-0.2
-0.3
-0.4
-0.5
-0.6
-0.7
0.0000000001
0.000000001
0.00000001
0.0000001
0.000001
0.00001
0.0001
A/cm^2

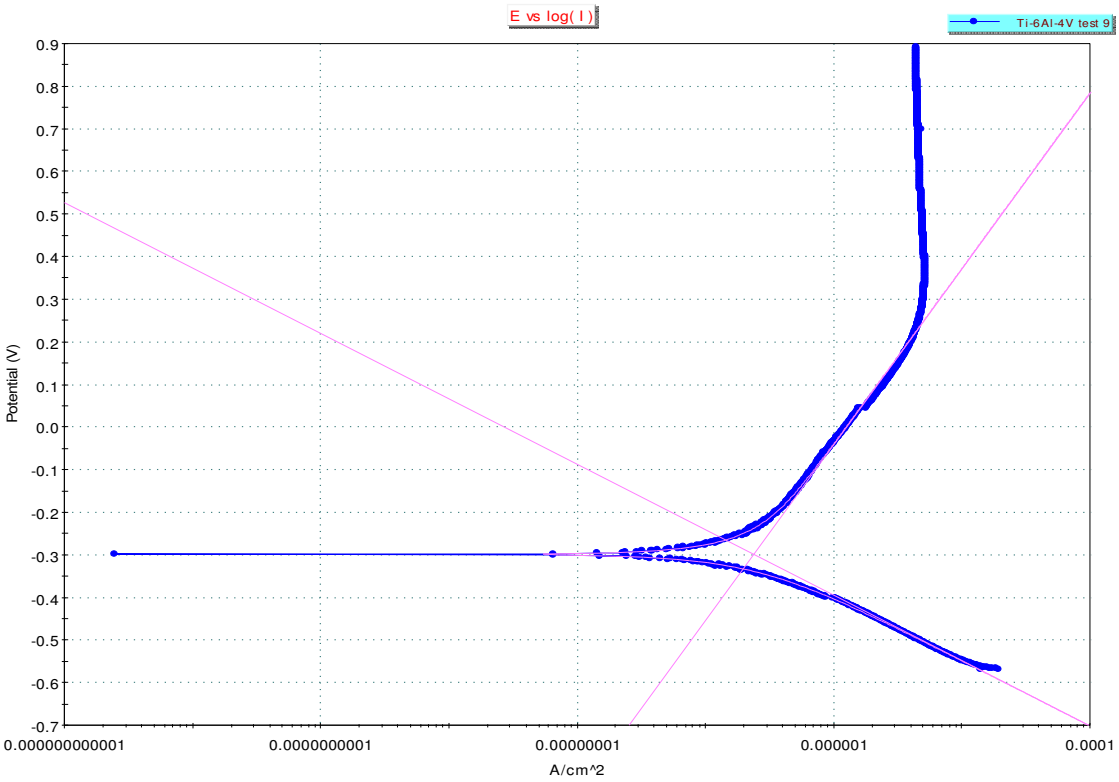
E vs log(I)
Ti-6Al-4V test 9
Potential (V)
0.9
0.8
0.7
0.6
0.5
0.4
0.3
0.2
0.1
0.0
-0.1
-0.2
-0.3
-0.4
-0.5
-0.6
-0.7
0.000000000001
0.0000000001
0.00000001
0.000001
0.0001
A/cm^2